catalysts

MDPI

Review

Recent Progress of 2D Pt-Group Metallic Electrocatalysts for Energy-Conversion Applications

Ziyue Chen, Yuerong Wang, Haiyan He and Huajie Huang *

College of Materials Science and Engineering, Hohai University, Nanjing 210098, China
* Correspondence: huanghuajie@hhu.edu.cn

Abstract

With the rapid growth of energy demand, the development of efficient energy-conversion technologies (e.g., water splitting, fuel cells, metal-air batteries, etc.) becomes an important way to circumvent the problems of fossil fuel depletion and environmental pollution, which motivates the pursuit of high-performance electrocatalysts with controllable compositions and morphologies. Among them, two-dimensional (2D) Pt-group metallic electrocatalysts show a series of distinctive architectural merits, including a high surface-to-volume ratio, numerous unsaturated metal atoms, an ameliorative electronic structure, and abundant electron/ion transfers channels, thus holding great potential in realizing good selectivity, rapid kinetics, and high efficiency for various energy-conversion devices. Considering that great progress on this topic has been made in recent years, here we present a panoramic review of recent advancements in 2D Pt-group metallic nanocrystals, which covers diverse synthetic methods, structural analysis, and their applications as electrode catalysts for various energy-conversion technologies. At the end, the paper also outlines the research challenges and future opportunities in this emerging area.

Keywords: Pt-group metals; nanosheets; electrocatalysts; controllable synthesis; energy-conversion



Academic Editor: John M. Vohs

Received: 29 June 2025
Revised: 23 July 2025
Accepted: 24 July 2025
Published: 27 July 2025

Citation: Chen, Z.; Wang, Y.; He, H.; Huang, H. Recent Progress of 2D Pt-Group Metallic Electrocatalysts for Energy-Conversion Applications. *Catalysts* **2025**, *15*, 716. https://doi.org/10.3390/catal15080716

Copyright: © 2025 by the authors. Licensee MDPI, Basel, Switzerland. This article is an open access article distributed under the terms and conditions of the Creative Commons Attribution (CC BY) license (https://creativecommons.org/licenses/by/4.0/).

1. Introduction

With the advent of the era of digital civilization, the global demand for energy has increased rapidly to meet the convenience of modern daily life [1,2]. In order to solve the problem of the depletion of fossil fuel resources and the ensuing environmental pollution, advanced energy-conversion technologies (e.g., water splitting, fuel cells, metal–air batteries, etc.) have attracted extensive attention from both academic and industrial fields [3,4]. Compared with the traditional internal combustion engine, the electrochemical systems based on the above new technologies are able to convert or generate energy with extremely high efficiency and low greenhouse gas emissions [5,6]. In particular, electrocatalysts play a key role as the core component of these energy-conversion devices, as they improve the selectivity, reaction rate, and overall efficiency [7–9]. However, the limited activity and poor stability of conventional electrocatalysts have severely hindered their large-scale applications [10–12]. Therefore, the major challenge is to develop advanced electrocatalysts and improve their performance to enable the widespread application of clean energy technologies [13–15].

Pt-group metals (e.g., Pt, Pd, Rh, Ru, Ir, etc.) have long been regarded as the mainstream electrocatalysts of current energy-conversion systems because of their superior catalytic capacity arising from the unique d-band structure [16–19]. Nevertheless, given

that the high costs and scarcity of Pt-group metals constrain their large-scale commercialization, great emphasis has been placed on developing optimization strategies to enhance both their catalytic activity and atomic utilization efficiency [20–22]. Therefore, great efforts have been devoted to the development of nanostructured Pt-group metallic nanocrystals [23–25]. Typically, most commercial electrocatalysts are made from small Pt-group metallic nanoparticles supported by carbon black matrices, which can increase the metal dispersibility and electroactive surface areas [26,27]. However, zero-dimensional (0D) Pt-group nanoparticles with large surface free energy easily suffer from agglomeration, dissolution, and Ostwald ripening phenomena during their practical use, resulting in an obvious deterioration in the electrocatalytic properties [28–30]. In the meantime, the limited contact area between particle-shaped Pt-group metals and carbon substrate through the "particle-to-face" contact model also renders a relatively weak synergistic coupling effect, which largely restrains the performance improvements [31–33]. Within this context, the rational design and precise synthesis of multi-dimensional Pt-group metallic nanocrystals with various controlled morphologies have become a hot topic in the field of electrocatalysis [34–36].

Since the successful exfoliation of graphene in 2004, two-dimensional (2D) materials have become a hot research topic over the last couple of decades due to their excellent electrical, magnetic, optical, mechanical, and thermal properties [37,38]. Researchers' exploration of novel 2D nanomaterials has significantly enriched the library of such materials, including transition metal disulfides (TMDs), MXenes, hexagonal boron nitride (h-BN), metal–organic frameworks (MOFs), covalent organic frameworks (COFs), metals, metal oxides, metal hydroxides, and so on [39,40]. These materials find applications across electronics, petroleum, chemical industries, aerospace, military, pharmaceuticals, medicine, and pharmaceutics [41–43]. As an important subset of 2D materials, 2D Pt-group metallic nanomaterials have garnered widespread attention in recent years [44,45]. Specially, the ultrathin 2D Pt-group metallic nanocrystals with a high surface-to-volume ratio commonly provide maximal exposure of active sites as well as minimize the charge transfer and mass diffusion pathways, thereby enhancing the atom utilization efficiency and electrocatalytic kinetics [46,47]. Moreover, the unique 2D morphology typically features undercoordinated metal atoms, which confer high chemical reactivity [48,49]. It is also noted that the adsorption strength of reaction intermediates on the catalyst surface should fall within the optimal "volcano" range based on Sabatier's principle [50,51]. Both overly strong and overly weak adsorption can impair overall catalytic performance [52,53], which puts requirements on the rational architectural design of 2D Pt-group metallic catalysts. On the other hand, the combination of Pt-group metallic nanosheets with nanocarbon supporting materials can form a 2D/2D heterostructure through a "face-to-face" contact model [54,55]. Such a sophisticated configuration has been demonstrated to effectively stabilize the Pt-group metal/carbon integral structure and generate extra concerted effects, thus affording a prolonged durability and boosted catalytic reactivity [56,57].

In the past few years, significant advances have been achieved in the design and fabrication of 2D Pt-group metallic nanocrystals, which have been extensively employed as electrocatalysts for diverse energy-conversion technologies [58,59]. Considering the fast-growing attention on this aspect, here, we intend to systematically summarize the latest advancements in this emerging field. As presented in Figure 1, this review first outlines diverse synthetic strategies of 2D Pt-group metallic electrocatalysts and discusses their respective characteristics and applicability. Afterwards, we highlight the electrocatalytic performances of various 2D Pt-group metallic nanocrystals towards different energy-conversion applications, including hydrogen evolution reactions (HERs), oxygen evolution reactions (OERs), oxygen reduction reactions (ORRs), formic acid oxidation reactions (FAORs), and alcohol oxidation reactions (AORs). To finalize, this review also proposes the

current challenges and opportunities associated with 2D Pt-group metallic electrocatalysts and provides a perspective for future research.

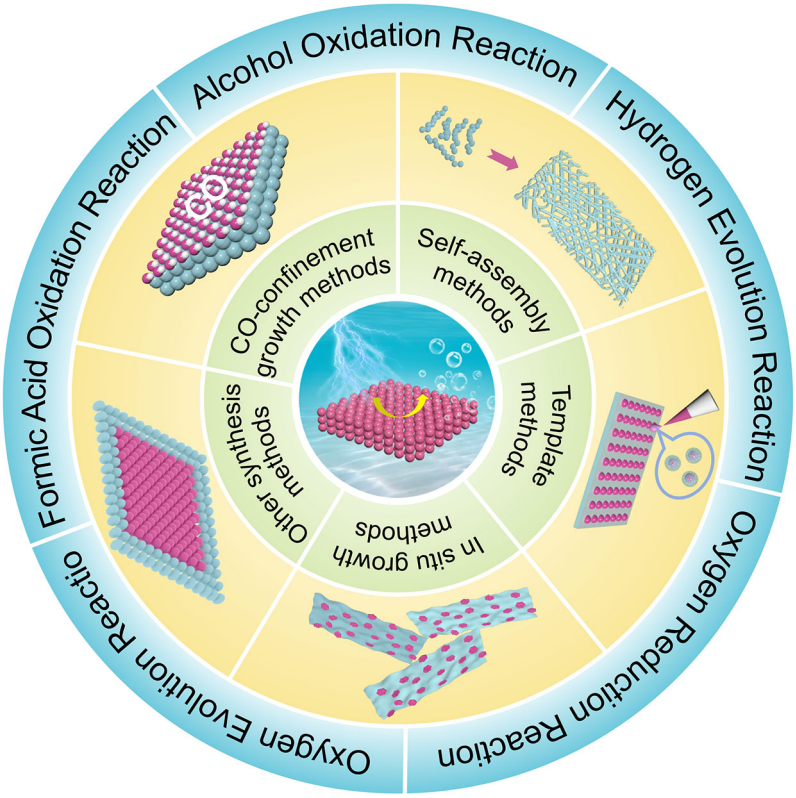


Figure 1. Schematic of 2D Pt-group metallic electrocatalysts synthesized by diverse methods and their applications for energy conversion.

2. Synthesis of 2D Pt-Group Metallic Electrocatalysts

To date, great efforts have been made to explore efficient synthesis strategies for the construction of 2D Pt-group metallic electrocatalysts [60,61]. These methods can be broadly classified into five categories: carbon monoxide (CO)-confined growth methods, self-assembly methods, template methods, in situ growth methods, and other synthesis methods [62,63]. In this section, we focus on the synthetic processes and growth mechanisms of various 2D Pt-group metallic electrocatalysts based on the above five strategies.

2.1. CO-Confined Growth Methods

The use of CO as a surface ligand to achieve the confined growth of 2D Pt-group metallic nanocrystals has emerged as an efficient synthetic method rooted in solution chemistry [64–66]. Typically, Pt-group metal atoms tend to form densely packed three-dimensional (3D) structures, which necessitate strong binding forces to inhibit their growth and stacking [67,68]. In this respect, CO functions as an effective capping agent to facilitate the attainment of 2D Pt-group metallic nanostructures by preferentially binding to the (111) facets of metal atoms [69,70]. As a typical example, Huang et al. conducted a pioneering study on the fabrication of free-standing hexagonal Pd nanosheets by utilizing CO as a surface capping agent [71]. Building upon this foundational work, Zhao's group successfully prepared ultrathin hexagonal Pd nanosheets with three different sizes by utilizing CO as a surface capping agent [72]. It was observed that a surface remodeling phenomenon occurred during the electrocatalytic reduction of CO_2 by defect-rich ultrathin Pd nanosheets. As illustrated in Figure 2a–c, the morphology of the ultrathin-sheet layer remained almost unchanged, while some nanopores penetrated the basal surface. Interestingly, the pristine

Pd nanosheets with major Pd(111) crystalline sites were then transformed into wrinkled lamellar structures prevalent in electrocatalytically active Pd(100) sites. In another work, Zheng's group prepared freestanding Rh nanosheets with long edge lengths from 500 to 1300 nm by adjusting the CO pressure in the range of 0.5–2.0 atm [73].

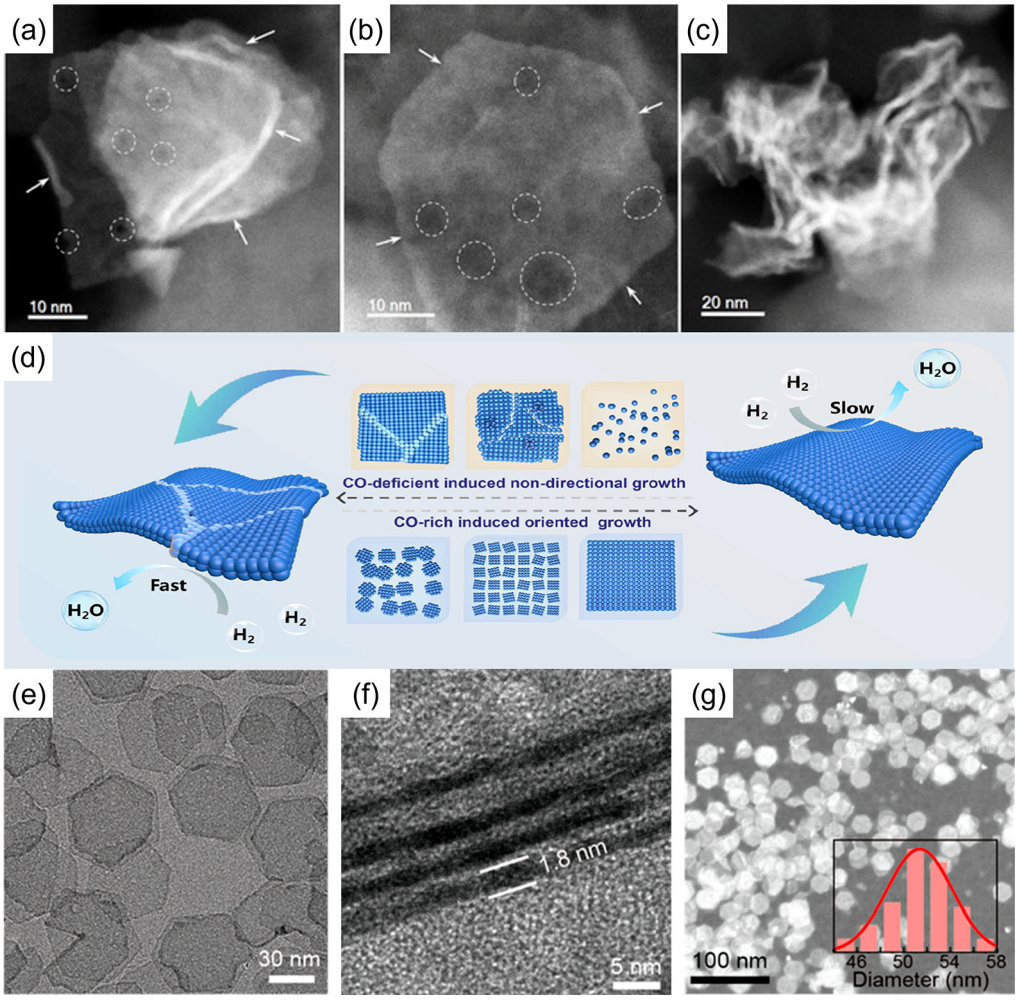


Figure 2. (**a**–**c**) HAADF-STEM images of 50 nm Pd NSs after electrolysis at −0.7 V for 300 s, 1500 s, and 3000 s (from ref. [72], with permission); (**d**) a roadmap for the synthesis of a series of Rh-based nanocrystals (from ref. [74] with permission); (**e**) plane-view and (**f**) side-view TEM images of stacked Pd nanosheets; (**g**) low-magnification STEM images. (Inset) Size distribution of the lateral sizes estimated from 100 images (from ref. [75] with permission).

In addition, a series of carbonyl-containing compounds, such as formaldehyde, $Mo(CO)_6$, $W(CO)_6$, and so on, were also employed to release CO molecules for the preparation of 2D Pt-group metallic nanoarchitectures [76,77]. For instance, Yang et al. successfully synthesized ultrathin Rh nanosheets with abundant grain boundaries with the help of formaldehyde by a kinetic control synthesis method [74]. As depicted in Figure 2d, the reduction of polyvinylpyrrolidone (PVP)-coordinated Rh^{3+} ions by formaldehyde initially yielded Rh nanoparticles, which could be further converted to grain-boundary-rich Rh nanosheets by the controlled release of CO through the in situ decomposition of formaldehyde. In another work, Wang and his collaborators successfully constructed an ultrathin curved Pd-Cu bimetallene with a thickness of 1.82 nm, during which the in situ-generated CO from the decomposition of *N*,*N*-dimethylformamide could facilitate the growth of the 2D structure [78]. The ultrathin curved geometry and the bimetallic composition effectively modulate the local chemical environment, thereby exposing sufficient active sites

and optimizing the oxygen adsorption energy. Similarly, the controllable construction of diverse 2D Pt-group metal-based alloy nanostructures, including PdCu, PdCo, PdPtNi, and PdPtMoCrCoNi nanosheets, was also realized using various carbonyl-containing compounds [79–82].

Although the use of CO gas and metal carbonyl compounds exhibits considerable potential for the confined growth of 2D Pt-group metallic nanocrystals, their implementation typically necessitates specialized laboratory equipment and stringent reaction conditions or presents an inherent risk of metal impurity contamination [83,84]. To address these issues, Ando et al. developed a green synthesis strategy employing 2,4,6-trichlorophenyl formate (TCPF) as an organic CO precursor [75]. In this synthetic process, the urea-derived ammonia would facilitate the in situ CO gas generation within the TCPF framework, which could serve both as a reducing agent and a surface-capping agent to effectively suppress oxide formation and impurity contamination, thereby enabling the high-yield synthesis of "clean" Pd nanosheets with a narrow size distribution (Figure 2e–g).

2.2. Self-Assembly Methods

Self-assembly is a highly versatile method for constructing nanostructured functional systems from a diverse array of small structural units [85,86]. The self-assembly process enables precise control over the composition, coordination environment, and nanoscale structure of catalysts, facilitating the optimization of their catalytic activity [87,88]. In recent years, self-assembly methods have been widely used to create various 2D Pt-group metallic nanoarchitectures with desired morphologies and compositions [89,90].

For example, Zu et al. synthesized a series of 2D iridium-based nanosheets through a nanoconfined self-assembly strategy utilizing block copolymers with stabilized ends embedded in lamellar micelles [91]. As shown in Figure 3a, the self-assembly process was initially performed to form lamellar organic–inorganic composite micelles, and then the residual tetrahydrofuran and water were evaporated at 100 °C to obtain organic–inorganic PS_{197}-b-PEO_{114}/Ir composites. Different lamellar micellar composites were prepared by adjusting the mass ratios of Ir^{3+}/PS_{197}-b-PEO_{114}. Finally, the ordered mesoporous Ir-IrO_x/C catalysts were in situ generated after calcination in an argon atmosphere. Remarkably, these nanosheets featured highly ordered interlayer channels (~20 nm) and uniformly distributed Ir-IrO_x nanoparticles (~2 nm) (Figure 3b–e), affording numerous catalytically active centers. In another study, Xie's group demonstrated the efficient synthesis of lamellar-assembled PdNi super-nanosheets with optimized Pd/Ni molar ratios by a controllable self-assembly method [92]. It was found that the resulting product showed a bunched-nanosheet structure comprising spontaneously lamellar stacking of several thin nanosheets (Figure 3f,g), which not only possessed enhanced stability and improved electron and mass transfer rates but also ensured a large surface area due to the layer-by-layer hierarchical nanostructure. Furthermore, Tang's group proposed a facile one-pot simultaneous step-by-step self-assembly synthesis strategy to prepare self-supported porous Pd nanosheets composed of crosslinked ultrathin nanowires assisted by poly(diallyldimethylammonium chloride) [93]. As shown in Figure 3h,i, the lateral size of the obtained Pd nanosheets was up to about 2.5 μm, and the corresponding thickness was around only 10 nm. Additionally, it was discovered that different dimensions of Pd nanostructures (including 3D nanoflowers, 2D nanosheets, and 1D nanochains) could be prepared by precisely controlling the pH values of the precursor solution.

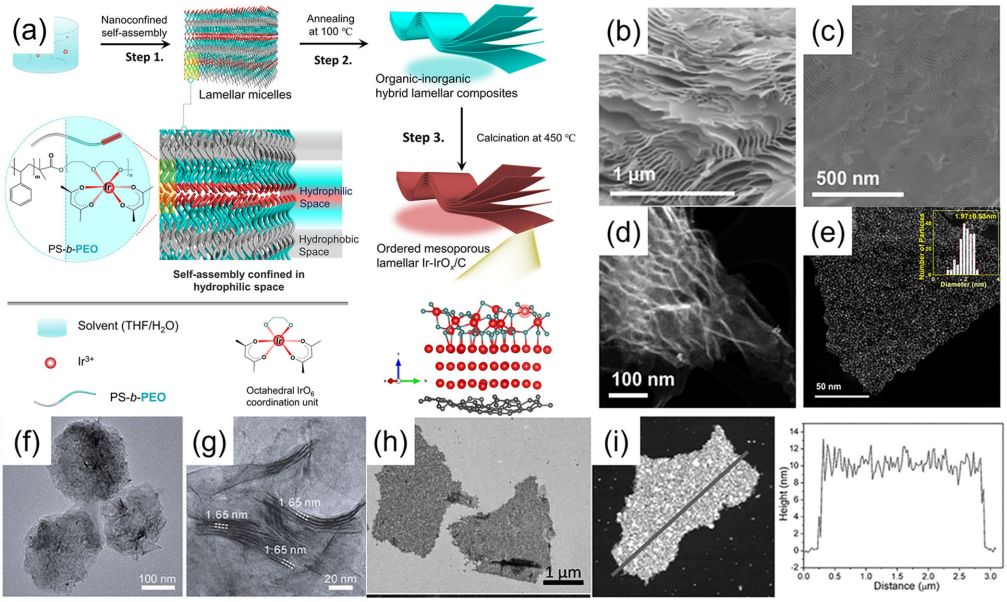


Figure 3. (**a**) Illustration of the formation of ordered mesoporous lamellar Ir-IrOx/C catalysts via the nanoconfined self-assembly approach; (**b**) SEM; (**c**) cross-section SEM; (**d**,**e**) low-magnification HAADF-STEM images of Ir-based nanosheets (from ref. [91] with permission); (**f**,**g**) TEM images of $Pd_{92}Ni_8$ SNSs (from ref. [92] with permission); (**h**) TEM, (**i**) AFM images and corresponding height profiles of Pd nanosheets (from ref. [93] with permission).

2.3. Template Methods

Template methods have long been regarded as an easy-to-use strategy that employs a template as the primary configuration to control, influence, and alter the shapes and sizes of Pt-group metallic nanocrystals [94–96]. The metal component is commonly deposited into the pores or onto the surface of the template by physical or chemical means, after which the template is removed to obtain the desired metallic forms [97,98]. One important contribution was that Li et al. demonstrated the template synthesis of self-standing mesoporous Pt nanosheets [99]. As illustrated in Figure 4a, solvent evaporation was used to induce the orderly self-assembly of spherical micelles composed of poly (styrene-b-2-vinylpyridine-b-ethylene oxide), which were confined within an ultrathin layer across the entire substrate surface. Afterwards, metal Pt deposition around the micelles was accomplished by a two-step reduction process utilizing two different reducing agents. After the removal of the micelles and the substrate, continuous self-standing ultrathin mesoporous Pt nanosheets (~15 nm thick) were obtained (Figure 4b,c).

Xu et al. demonstrated the facile powerful bottom-up synthesis of ultrathin Pd nanosheets (PdNS) with efficiently controlled surface facets through a template-assisted solution-phase growth [100]. By modulating the head group functionality of surfactants, PdNSs with exposed low-index {100}, {110}, and {111} facets were selectively produced. Consequently, PdNS{100} demonstrated superior electrocatalytic activity and stability relative to PdNS{110} and PdNS{111}. In addition, Yamamoto and co-workers pioneered a new template method for synthesizing molecularly thin Pt metal nanosheets using solid surfactant crystals as precursors [101]. They first prepared the surfactant crystals with planarly arranged Pt complexes and subsequently controlled the morphology and thickness of 2D surfactant crystals by recrystallization followed by a UV-ozone treatment and reduction process under H_2/Ar flow. As a result, the derived Pt metal nanosheets exhibited varying thicknesses ranging from 1.5 to 3.0 nm while retaining the structural features of the 2D surfactant crystals.

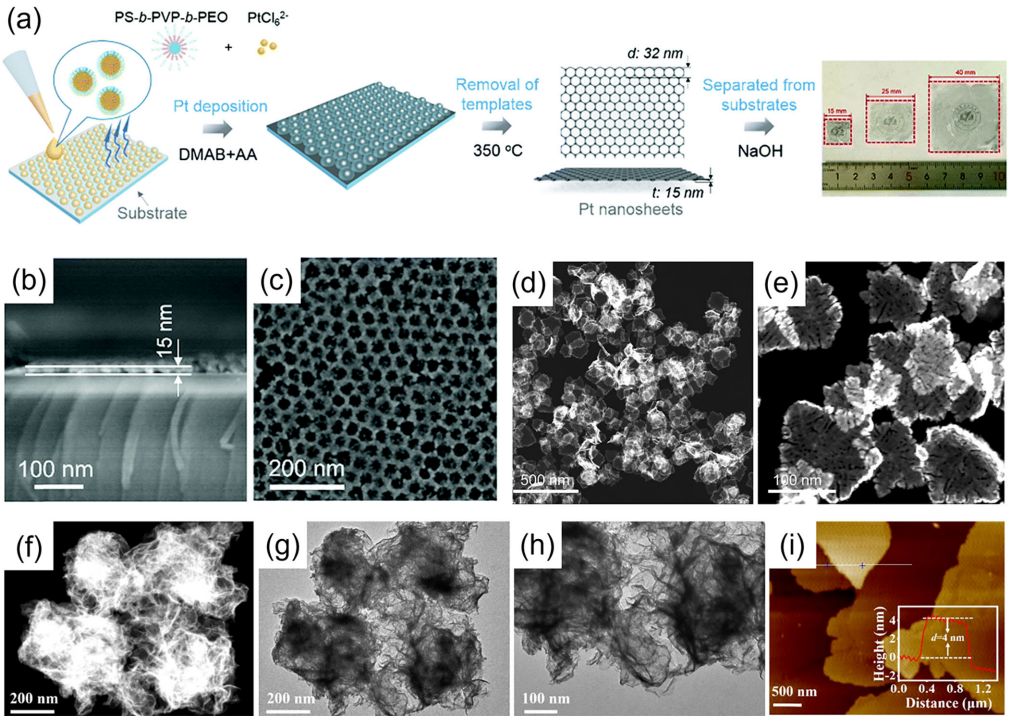


Figure 4. (**a**) Illustration describing the synthesis of the meso-Pt nanosheets; (**b**) cross-section SEM and (**c**) top-view SEM of the meso-Pt nanosheets (from ref. [99] with permission); (**d**,**e**) HAADF-STEM images of PdAg nanosheets at different resolutions (from ref. [102] with permission); (**f**) HAADF-STEM, (**g**,**h**) TEM and (**i**) AFM images of the PdRhBP nanosheets (from ref. [103] with permission).

In order to further improve the catalytic ability of 2D Pt-group metallic electrocatalysts, multi-element synergistic template strategies have also been developed. As an example, Teng et al. utilized lamellar micelles as soft templates to chemically constrain the growth of the 2D Pd structure and simultaneously employed silver as a co-metal to modulate the reduction kinetics of Pd nanocrystals [102]. The prepared PdAg nanosheets displayed a homogeneous and monodisperse sheet-like nanostructure with an average lateral diameter of 150 nm (Figure 4d). Unlike the traditional nanosheets with smooth and intact surfaces, PdAg nanosheets showed a snowflake-like morphology with abundant active dendrites (Figure 4e). Li and co-workers successfully prepared B and P co-doped PdRh (PdRhBP) nanosheets by using pre-synthesized PdRh nanosheets as the compositional templates, as well as $NaBH_4$ and NaH_2PO_2 as the B and P sources, respectively [103]. The resultant quaternary PdRhBP material could not only completely preserve the 2D morphology of the pristine PdRh nanosheets to form an ultrathin curled structure (Figure 4f–i) but could also optimize the electronic structure of the catalytically active sites through the synergistic effects of multiple elements. To address the difficulties of the traditional template method such as the residual surfactant blocking the active site, Lee's group employed Ni-Fe layered double hydroxides (LDHs) as a 2D substrate to prepare 2D Pt nanostructures with ligand-free clean catalytic surfaces [104]. This design strategy endowed the resulting hybrid catalyst with surfactant-free and atomically ultra-exposed heterointerfaces, which were beneficial in increasing the Pt-atom utilization efficiency.

2.4. In Situ Growth Methods

The in situ growth of 2D Pt-group metallic nanocrystals onto advanced supporting materials with large surface area and high electrical conductivity is also an efficient strategy to reduce the precious metal loading as well as stabilize their thin-sheet nature [105–107]. Among the various carbonaceous matrixes, graphene or reduced graphene oxide (RGO)

has been recognized as a superior substrate for the growth and dispersion of diverse 2D Pt-group metallic nanostructures [108]. For instance, Yang et al. achieved the preparation of ultrathin PdMo bimetallene in situ immobilized on the RGO carrier through a robust stereo-assembly procedure [109]. As seen from Figure 5a–d, the highly-curved PdMo bimetallic nanolayers were almost transparent, which were uniformly distributed on the RGO nanosheets through direct "face-to-face" contact. Notably, the presence of PdMo bimetallene on the RGO substrate effectively prevented the nanosheets from restacking, and this unique 2D/2D heterostructure provided multiple catalytically active sites. In another work, He et al. proposed a solid-phase synthesis method to produce 2D ultrathin Pd and its alloy nanosheets (PdFe, PdCo and PdNi) on the RGO carrier [110]. TEM observation revealed that thin Pd nanosheets with rich jagged edges were flatly laid on the RGO support with an average size of about 20 nm. In comparison with the conventional wet-chemical synthetic route, the solid synthesis of these Pd-based nanosheets did not require the use of any templates or surfactants, and in the meantime, the catalysts could be produced in larger quantities.

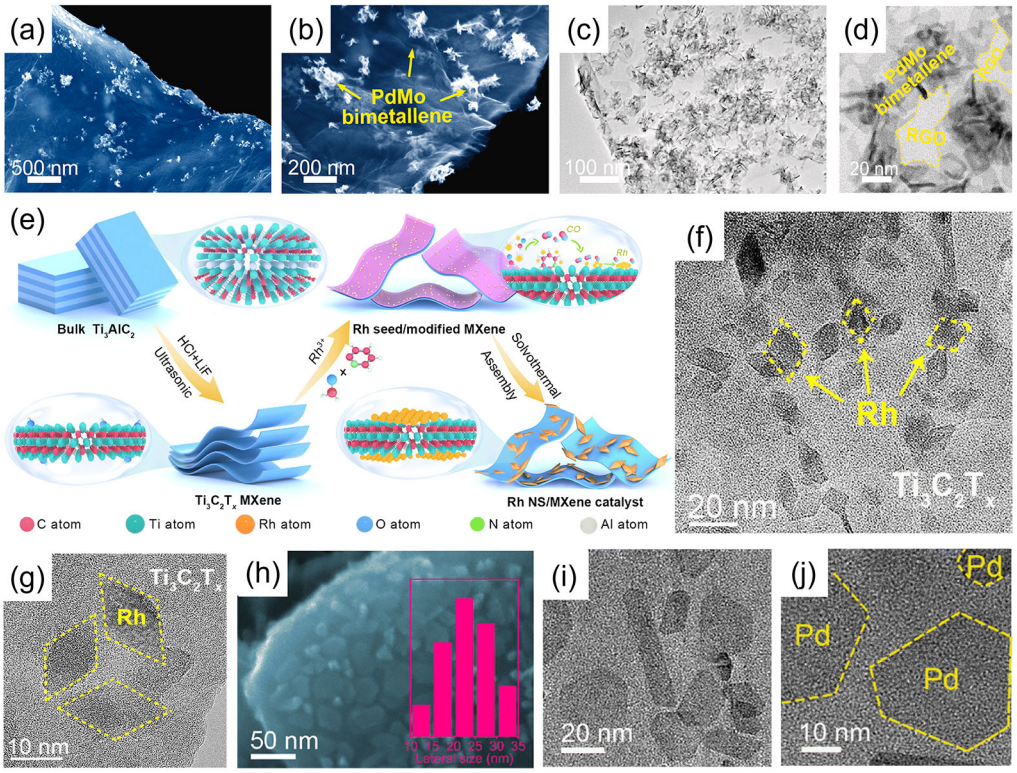


Figure 5. (**a**,**b**) FE-SEM and (**c**,**d**) TEM images of PdMo bimetallene on RGO nanosheets (from ref. [109] with permission). (**e**) The synthesis process of the Rh nanosheets/MXene nanoarchitectures. (**f**,**g**) TEM images of Rh nanosheets/MXene. The inset in (**g**) is the Rh size distribution (from ref. [111] with permission). (**h**) FE-SEM and (**i**,**j**) TEM images of Pd nanosheets/MXene. The inset in (**h**) is the corresponding Pd lateral size distribution (from ref. [112] with permission).

Over the past few years, 2D transition-metal carbides/nitrides (MXene) have shown great potential to serve as a novel matrix for the confined growth of various Pt-group metallic nanocrystals because of their large accessible surface areas, tunable termination groups, good hydrophilic properties, and high metallic conductivity [113–115]. Typically, our group presents a robust and convenient wet-chemical approach for the construction of a 2D/2D heterojunction consisting of ultrathin Rh nanosheets in situ grown on $Ti_3C_2T_x$ MXene [111]. As shown in Figure 5e, 2D $Ti_3C_2T_x$ MXene nanolayers were first produced from bulk Ti_3AlC_2 MAX powder using a LiF and HCl etching route, followed by the growth

of Rh seeds on the MXene surface. Afterward, formaldehyde was decomposed to generate plentiful CO molecules with the assistance of pyridine, resulting in the gradual formation of 2D Rh nanosheets on MXene nanoflakes. The generated Rh nanosheets were rhombic in shape with sizes between 10 and 15 nm, which could provide abundant unsaturated Rh atoms with optimized electronic structure (Figure 5f,g). Furthermore, we recently reported the successful fabrication of $Ti_3C_2T_x$ MXene-supported Pd nanosheets via a heterointerface engineering strategy that involves the decomposition of $Mo(CO)_6$ to produce CO molecules. As seen from Figure 5h–j, most Pd nanosheets appeared as a regular hexagonal shape with sizes between 10 and 35 nm, which were intimately attached to the MXene matrix through a strong atomic interaction at the heterointerfaces [112].

2.5. Other Synthesis Methods

Besides the aforementioned four principal strategies, other synthesis methods have also been developed for the construction of 2D Pt-group metallic electrocatalysts. For example, the epitaxial growth method involves the deposition of atoms from a thin crystalline layer onto a single-crystal substrate, thereby replicating the substrate's atomic arrangement and yielding high-quality interfaces [116]. In a typical study, Du's group reported an epitaxial seed growth method to build a 2D heterostructure consisting of Pt nanoparticles grown on Pd nanosheets [117]. Notably, a rapid reduction kinetic could make the Pt nanoparticles evenly deposited on the Pd nanosheets, while a slow reduction kinetic led to the preferential growth of Pt nanoparticles on the edges of Pd nanosheets (Figure 6a–c). Density functional theory (DFT) calculations showed that the Pd(111)–Pt interfaces induced a more pronounced electron-deficient state of Pd carriers, affording a lower-band center and stronger intermetallic interaction.

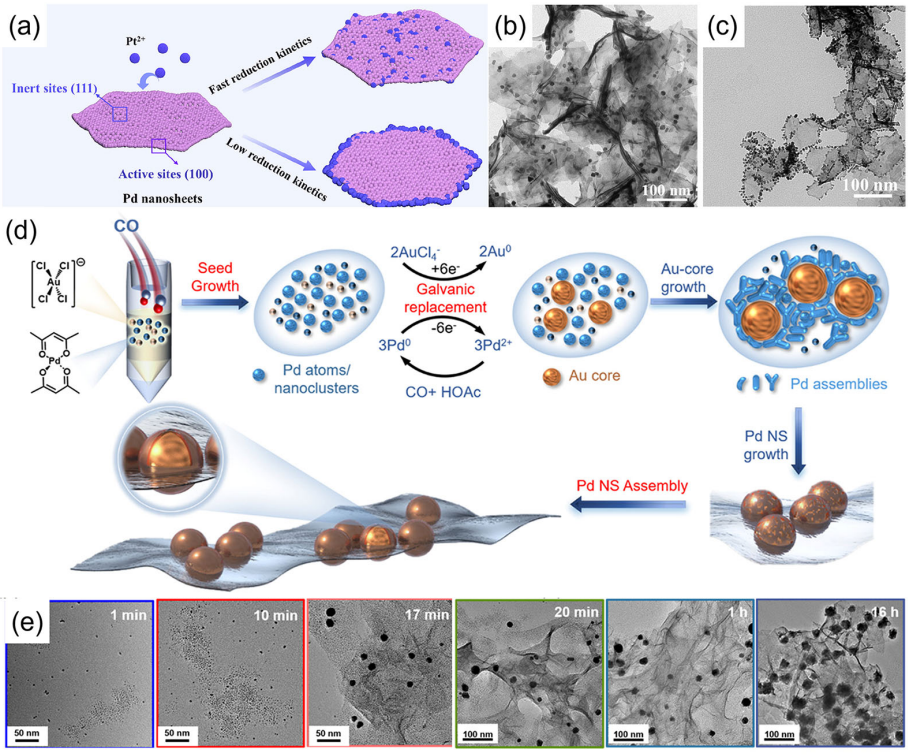


Figure 6. (**a**) The synthesis process of Pt NPs on Pd NSs; (**b**) TEM image of U-Pd@Pt HS; (**c**) TEM image of E-Pd@Pt HS (from ref. [117] with permission). (**d**) The synthesis process of 2D AuNP-in-PdNS heterostructure; (**e**) ex situ TEM characterization of AuNP-in-PdNS heterostructures (from ref. [118] with permission).

Another interesting advance is that Ding et al. designed a new 2D heterostructure with Au nanoparticles intercalated in Pd nanosheets via a facile wet chemical method combining seed growth, plating substitution and assembly in a single step (Figure 6d) [118]. It was found that most Au particles were not coated on the Pd nanosheets but buried within the body of Pd nanosheets. As shown in Figure 6e, a large number of spherical Au nanoparticles with a diameter of ~15 nm were intercalated within ultrathin Pd nanosheets to form an interesting egg-waffle-like morphology, which contributed to efficient hot-carrier generation that could mediate a direct transfer of plasmonic energy to the metal-adsorbate complex.

3. Applications of 2D Pt-Group Metallic Electrocatalysts for Energy Conversion

Two-dimensional Pt-group metallic nanocrystals have become a research hotspot in the field of electrocatalysis due to their attractive architectural features, including atomic-level thin-layer structure, large specific surface area, and plenty of unsaturated ligand atoms. As core components of novel energy-conversion devices, electrode catalysts play crucial roles in boosting the reaction efficiency and improving the overall output power [119–123]. In this section, the recent advances on the development of 2D Pt-group metallic nanocrystals as electrocatalysts are systematically summarized and discussed based on five typical electrocatalytic reactions, including hydrogen evolution reaction (HER), oxygen evolution reaction (OER), oxygen reduction reaction (ORR), formic acid oxidation reaction (FAOR), and alcohol oxidation reaction (AOR).

3.1. Hydrogen Evolution Reaction

Electrochemical water splitting has been widely recognized as a highly promising hydrogen production technology due to its advantages of high efficiency, environmental friendliness, and sustainability [124–126]. A typical electrolyzer system comprises three essential components: an electrolyte, an anode, and a cathode [127,128]. When an appropriate external voltage is applied to the electrodes, water molecules dissociate at the cathode to generate hydrogen gas, while oxygen evolves at the anode [129,130]. The cathodic half-reaction, known as the HER, constitutes the fundamental electrochemical process in electrocatalysis [131,132]. Similar to most electrochemical reactions, HER requires efficient catalysts to optimize the reaction kinetics and minimize the overpotential [133–135]. Currently, commercial HER electrocatalysts predominantly employ Pt-based materials, which dominate the field owing to their exceptional catalytic activity and ultralow overpotential, while their high costs severely limit large-scale commercial applications [136–138].

To address this issue, great efforts have been devoted to the exploration and utilization of 2D Pt-group metallic electrocatalysts, which show huge potential for cost reduction and HER performance improvement [139,140]. For example, Zhang and co-workers successfully prepared a series of ultrathin RuPdM (M = Ni, Co, Fe) nanosheets for the first time and investigated their HER activity [141]. As displayed in Figure 7a,b, optimized trimetallic RuPdNi nanosheets exhibited a unique 2D lamellar structure with an atomic-level thickness of about six atomic layers (≈1.6 nm) as well as uniform dispersions of Ru, Pd, and Ni throughout the whole nanosheets. Electrochemical tests revealed that the $Ru_{38}Pd_{34}Ni_{28}$ electrocatalyst required a low overpotential of only 20 mV at a current density of 10 mA cm^{-2}, superior to the widely used Pt/C and Pd/C catalysts. DFT calculations elucidated that the introduction of 3D transition metals (Fe, Co, and Ni) was able to induce the modulation of RuPd electronic structures to enhance the intrinsic catalytic activity.

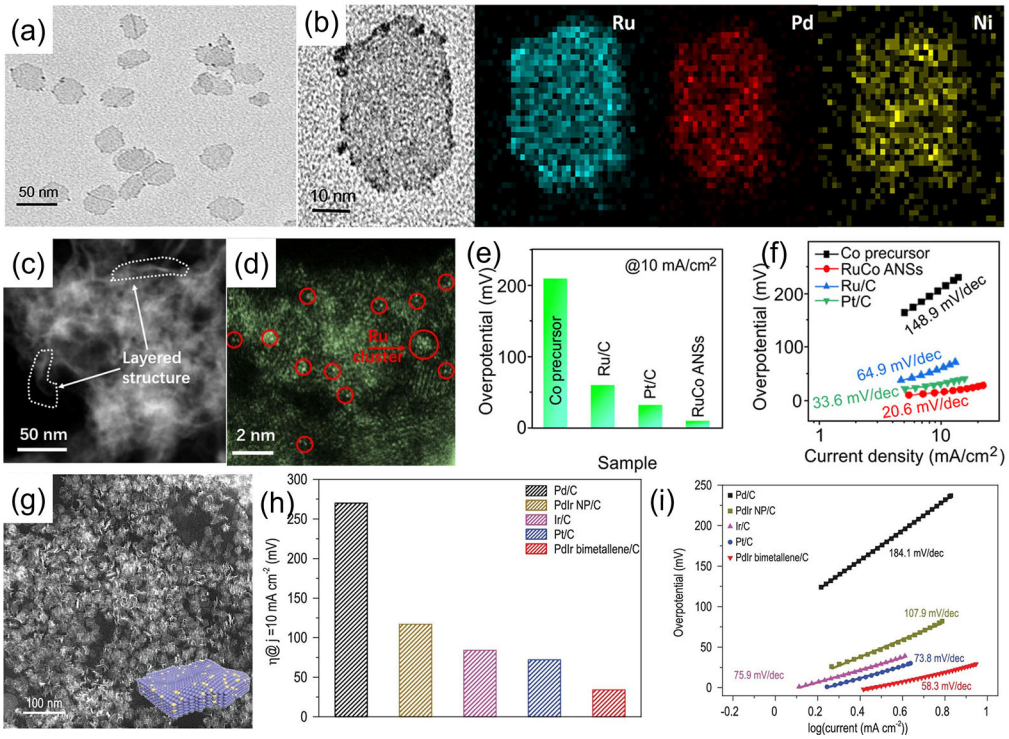


Figure 7. (**a**) TEM image and (**b**) corresponding TEM mapping image of $Ru_{38}Pd_{34}Ni_{28}$ ultrathin NSs (from ref. [141] with permission); (**c**) STEM image and (**d**) high-resolution STEM image of RuCo ANSs; (**e**) calculated overpotentials at 10 mA cm^{-2} and (**f**) Tafel plots of various catalysts (from ref. [142] with permission); (**g**) low-magnification HAADF-STEM image of PdIr bimetallene; (**h**) overpotentials at 10 mA cm^{-2} and (**i**) Tafel slopes of different catalysts (from ref. [143] with permission).

Moreover, Cai et al. demonstrated through DFT simulations that the essence of the Ru-H binding energy depended on the strong interaction between the $4dz^2$ orbital of Ru and the 1s orbital of H [142]. The charge transfer between the Ru and CoNi substrate caused the band center of Ru to shift downwards, which resulted in a suitable Gibbs free energy of 0.022 eV for H^* in the RuCo structure. To verify this prediction, RuCo alloy nanosheets with different proportions were prepared by a combined precipitation and electrochemical reduction process. It can be seen from Figure 7c–f that Ru atoms were embedded into the Co matrix to form an optimized coordination structure, which exhibited an ultra-low overpotential of 10 mV at a current density of 10 mA cm^{-2} and a small Tafel slope of only 20.6 mV/dec in the alkaline medium, more competitive than the commercial Pt/C catalyst. Jin et al. reported the fabrication of holey large-area 2D Ru nanosheets by the reductive phase transition of monolayer RuO_2 nanosheets [144]. Their study revealed that the metal coordination number was a critical parameter governing the catalytic HER performance of the resultant Ru nanosheets. With an optimal coordination number of Ru atoms of ~10.2, the holey metallic Ru nanosheets achieved a remarkably low overpotential of 38 mV at 10 mA cm^{-2} in the presence of 1 M KOH, outperforming that of bulk Ru metal and commercial 20 wt% Pt/C electrocatalysts.

Recent theoretical and experimental research has also demonstrated that the intrinsic strains in atomically thin 2D alloys are associated with their specific thickness or curvature, which is able to greatly modulate the surface electronic structure and energy of the reaction intermediates, thus promoting catalytic activity [145,146]. Specifically, tensile strains induce lattice expansion and thus weaken the interatomic interactions, which could lead to an upward shift of the center of the d-band and increase the adsorption energy between the absorbed molecules and the catalyst [147,148]. In contrast, compressive strains have the opposite effects, shifting the d-band center downward and decreasing the adsorption

energy between the catalysts and adsorbates [149,150]. According to the Sabatier principle, the optimal catalyst should have a reactant and intermediate adsorption energy that is neither too high nor too low [151,152], which implies that a suitable intrinsic strain is very beneficial to boost the catalytic efficiency of 2D Pt-group metallic electrocatalysts. Based on this, Guo's group proposed a novel strategy to synthesize ultrathin curved PdIr bimetallene with a thickness of about five atomic layers (Figure 7g) [143]. Theoretical simulations proved that the surface strain effects endowed the PdIr bimetallene with plenty of concave–convex featured electro-active regions. Accordingly, the PdIr bimetallene/C catalyst with a Pd/Ir atomic ratio of 4: 1 manifested the best HER performance with an overpotential of 34 mV at 10 mA cm^{-2} and a Tafel slope of 58.3 mV dec^{-1}, superior to the PdIr nanoparticle/C and Pt/C catalysts (Figure 7h,i). In addition, Yin et al. prepared curled and perforated PdIn bimetallene with abundant defective sites through a one-step solvothermal method, which exhibited excellent activity and stability for both HER and methanol oxidation reaction (MOR) [153]. In a typical MOR-HER co-electrolysis system assembled with the bifunctional PdIn bimetallene as both the anode and cathode, a current density of 100 mA cm^{-2} could be driven by a tank voltage of only 1.26 V, which was 0.93 V lower than that of a conventional water electrolysis system without methanol.

3.2. Oxygen Evolution Reaction

As another half reaction of electrochemical water splitting at the anode, the oxygen evolution reaction has also emerged as a promising energy-conversion technology for renewable hydrogen production [154,155]. Noteworthily, in comparison with the HER, the OER process exhibits inherently slower kinetics, primarily due to its complex four-electron transfer mechanism involving proton-coupled steps [156,157]. This kinetic limitation manifests as substantial overpotential requirements, which critically decreases the overall energy-conversion efficiency of the electrolysis system [158,159]. Consequently, the development of high-performance OER catalysts remains a key research focus for optimizing the performance of the electrochemical water splitting device [160,161].

Ir-based materials have been considered as the current state-of-the-art acidic OER catalysts due to their good stability under harsh acidic conditions [162,163]. However, the intrinsic activity of Ir-based catalysts is insufficient, which severely limits the OER efficiency [164,165]. To address this problem, researchers have focused on the morphological regulation of Ir-based catalysts with various 2D configurations, which have achieved a significant increase in catalytic activity [166,167]. As a typical example, Yamauchi's group developed a soft polymeric micelle template-assisted construction of 2D mesoporous Ir nanosheets and investigated their OER performance [168]. As presented in Figure 8a,b, the as-derived metallic Ir sample appeared to be an interconnected thin-sheet network, where a large number of mesopores with a diameter of around 15 nm were homogeneously distributed over whole nanosheets. By virtue of their unique architectural features, the mesoporous Ir nanosheets exhibited an unusual OER performance with a low overpotential of 240 mV at 10 mA cm^{-2} and a Tafel slope of 49 mV dec^{-1} in 0.5 M H_2SO_4 electrolyte, much better than that of commercial Ir black and IrO_2 catalysts (Figure 8c,d). In addition, Chatterjee and co-workers proposed the top-down synthesis of nanoporous Ir nanosheets for catalyzing the OER process [169]. As shown in Figure 8e,f, these Ir nanosheets have a lateral size of several microns, a thickness of about 100 nm, and rich porosity. Impressively, the nanoporous Ir nanosheets exhibited stable electrocatalytic properties over 50,000 accelerated stress test cycles in the polymer electrolyte membrane water electrolyzer (PEMWE) (Figure 8g). Yang's group prepared a hexagonal nanosheet structure with lattice distortion and edge-connected [IrO_6] octahedra to effectively improve the OER performance [170]. In 0.1 M $HClO_4$ electrolyte, the mass activity of this newly designed

catalyst was up to 217 mA mg_{Ir}^{-1} at 1.55 V, which was 13 times higher than that of rutile iridium dioxide.

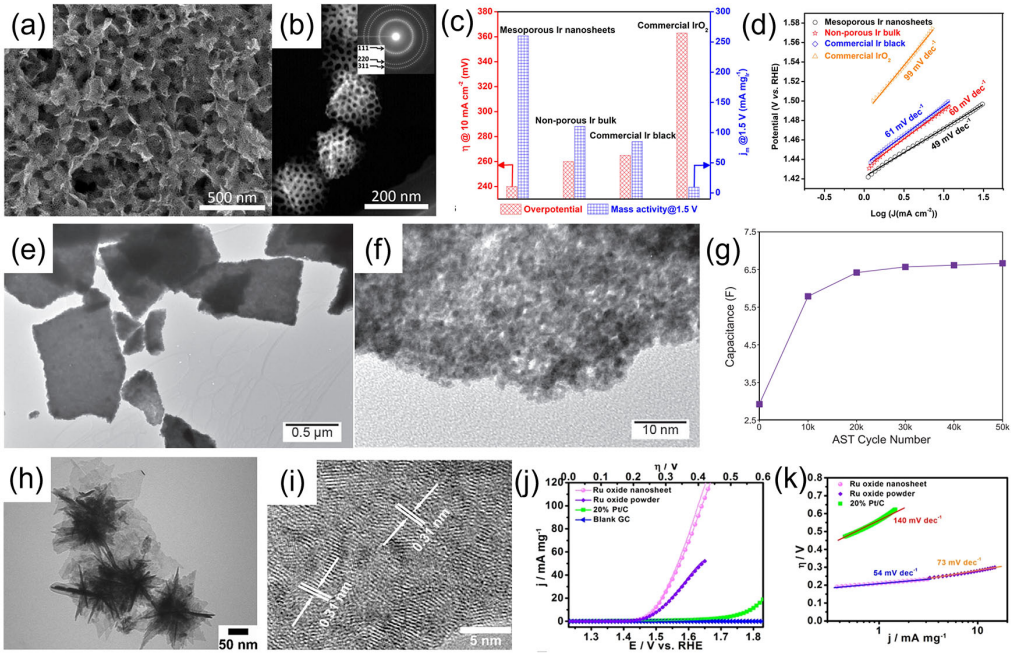


Figure 8. (**a**) Low-magnification SEM and (**b**) TEM images of mesoporous Ir nanosheets; (**c**) bar graph showing the overpotential to drive 10 mA cm^{-2} and Ir mass activity at 1.5 V (vs RHE); (**d**) Tafel plots of mesoporous Ir nanosheets versus nonporous Ir bulk, commercial Ir black, and IrO_2 catalysts as OER catalysts (from ref. [168] with permission); (**e**,**f**) TEM images of $npIr_x$-NS; (**g**) AST of $npIr_x$-NS (from ref. [169] with permission); (**h**) TEM and (**i**) HRTEM images of 2D Ru oxide derivative nanosheets; (**j**) LSV and (**k**) Tafel plots of Ru oxide nanosheets in OER (from ref. [171] with permission).

Considering that Ir is one of the rarest elements, with an annual production of only 5~8 tons, its limited supply can hardly meet the demand for large-scale development of PEMWE [172,173]. In this context, metallic Ru has recently been regarded as a promising Ir-alternative electrode catalyst for the OER in acidic conditions owing to its more abundant reserve and relatively lower cost [174,175]. For instance, Kong et al. reported the rational design and solvothermal production of 2D free-standing ultrathin Ru nanosheets with clean surfaces [171]. In particular, these Ru nanosheets were mildly heat-treated in the atmospheric environment to allow the conversion of metallic Ru surface to oxide form while maintaining their 2D thin-sheet structure for the OER application (Figure 8h,i). As shown in Figure 8j,k, the onset overpotential of the ruthenium oxide nanosheets was determined to be 220 mV, significantly better than that of commercial Pt/C (430 mV). In the meantime, an overpotential of only 260 mV was required for the Ru-based nanosheets to derive a current density of 10 mA mg^{-1}, which was lower than that required for the Ru powder catalyst. Furthermore, the current density increased exponentially with applied potential, and the corresponding Tafel plot analysis indicated that the Ru nanosheets exhibited the lowest Tafel slope of only 54 mV dec^{-1}. In addition, Yuan et al. proposed that a stable Pt_5Se_4 monolayer could be obtained from bulk Pt_5Se_4 crystals by mechanical exfoliation [176]. Surface Pt atoms in this monolayer exhibited quasi-neutral charge states analogous to Pt(111) surfaces. This electronic configuration may confer exceptional electrocatalytic properties. Regarding OER, the overpotential of monolayer Pt_5Se_4 was calculated to be 0.35 V, comparable to those of Ru and Ir oxide catalysts (0.37 and 0.56 V).

3.3. Oxygen Reduction Reaction

Proton exchange membrane fuel cells (PEMFCs) have been recognized as one of the core technologies for building a sustainable hydrogen energy system due to their high energy-conversion efficiency, zero pollution, low working temperature, and facile cell configuration, which have received extensive attention from both academia and industry in recent years [177,178]. In particular, the cathodic ORR is a crucial electrochemical process that directly influences the energy-conversion efficiency of PEMFCs [179,180]. Currently, the overall performance of PEMFCs has been largely limited by the slow kinetics of the ORR process [181,182]. As is known, Pt and Pt-derived electrocatalysts can effectively catalyze the ORR, but their high cost and insufficient stability have severely hindered the scalability of the PEMFC technology. In addition, low-buffering-capacity solutions can significantly change the local pH at the electrode/solution interface, which in turn affects the reaction path and kinetic rate, which can be visualized through the fluorescence imaging of the interface [183]. Therefore, the development of highly active and long-lasting ORR electrocatalysts has become a key challenge to promote the hydrogen economy and popularize clean energy technology [184,185]. Typically, the performance evaluation for Pt-based catalysts relies on a variety of electrochemical techniques: (1) hydrogen adsorption/desorption analysis via cyclic voltammetry (CV) using stationary catalyst-loaded electrodes to calculate the electrochemical surface area (ECSA); (2) CO stripping tests (following the DOE protocol) for ECSA calculation and anti-toxicity analysis; and (3) CV and linear sweep voltammetry (LSV) techniques for the assessment of mass activity and cycling stability [186,187]. In order to deeply analyze the electrocatalytic ORR mechanism, the rotating ring disk electrode (RRDE) coupled with online differential electrochemical mass spectrometry (DEMS) provides a powerful tool to reveal the reaction pathway by real-time monitoring of the reaction intermediates and gas products [188,189].

To enhance the catalytic ORR performance, researchers have developed a variety of Pt-group metallic nanosheet systems through various structural design concepts [190,191]. For example, Zhang and co-workers utilized microwave-assisted heating to deposit a significant number of Pt atoms into PdCu nanosheets to form a series of ternary PtPdCu nanosheets [192]. As presented in Figure 9a–d, the as-obtained ternary nanosheets possessed a 2D wavy nanostructure, where Pt, Pd, and Cu elements were uniformly distributed over the nanosheets. It was found that the PtPdCu alloy effects could induce the lattice distortion of Pt atoms, and the resulting compressive strain was essential to improving the ORR ability. As a result, the optimized $Pt_{38}Pd_{50}Cu_{12}$ nanosheet catalyst expressed the best catalytic optimized activity with an ECSA of 118.7 m^2/g_{Pt+Pd} and a mass activity of 0.93 A/mg_{Pt+Pd} at 0.9 V. After 10,000 cycles of an accelerated durability testing (ADT) cycling test, the $Pt_{38}Pd_{50}Cu_{12}$ catalyst exhibited an attenuation of only 9.2% in terms of ECSA and 11.4% in terms of mass activity. Additionally, the $Pt_{38}Pd_{50}Cu_{12}$ nanosheets also realized a maximum power density of 796 mW cm^{-2} in the single-cell test, far surpassing that of traditional Pt/C catalyst (606 mW cm^{-2}). Guo's group reported the construction of Pt-on-Pd dendritic nanosheets made from Pt branches grown in situ on the surface of ultra-thin Pd nanosheets (Figure 9e,f) [193]. Strikingly, the separate dendritic nanostructure could inhibit the clustering of the active sites and create electronic coupling effects between Pd-Pt bimetallic crystals, which effectively improved the catalytic ORR capacity. As depicted in Figure 9g, the specific activity and mass activity of Pt-on-Pd dendritic nanosheets were 3.0 and 2.2 times higher than those of a commercial Pt/C catalyst, respectively, accompanied by superior cycling performance.

Two-dimensional Pt-group metallic nanosheets with rich wrinkles have been proved to not only significantly improve the electrolyte penetration and transport but also inhibit the aggregation of metal nanolayers, commonly leading to enhanced electrocatalytic ORR

efficiency. In this aspect, Zhang et al. synthesized highly wrinkled Pd nanosheets with a bent cross-linked structure to increase the compressive strain for rapid electrocatalytic kinetics [194]. Consequently, the prepared highly wrinkled Pd nanosheets depicted excellent ORR properties in acidic media with 26 mV more positive half-wave potential and much better stability when compared with commercially available Pd/C and common Pd nanosheet catalysts. Theoretical simulations disclosed that the compressive strain arising from the wrinkles was able to downshift the d-band center of the Pd component, which could reduce the reaction barriers of the rate-determining step for the ORR process. As another example, Chen et al. successfully prepared ultrathin wrinkled FePt nanosheets decorated with high-density neighboring dispersed Pt atoms and investigated their ORR performance [195]. As shown in Figure 9h,i, the synthesized FePt nanosheets were only 1.2 nm thick and consisted of about 5–6 atomic nanolayers, along with numerous Pt atoms positioned on the wrinkled surface. Such a neighboring-atom electrocatalyst retained the merits of conventional single-atom catalysts and meanwhile was able to synergistically catalyze the reactions that require two or more neighboring sites. As a result, the wrinkled FePt nanosheets manifested a four-electron reduction pathway, a large electrochemical active surface area of 545.5 m^2 g^{-1}, stable mass activity, as well as good CO tolerance towards the ORR (Figure 9j).

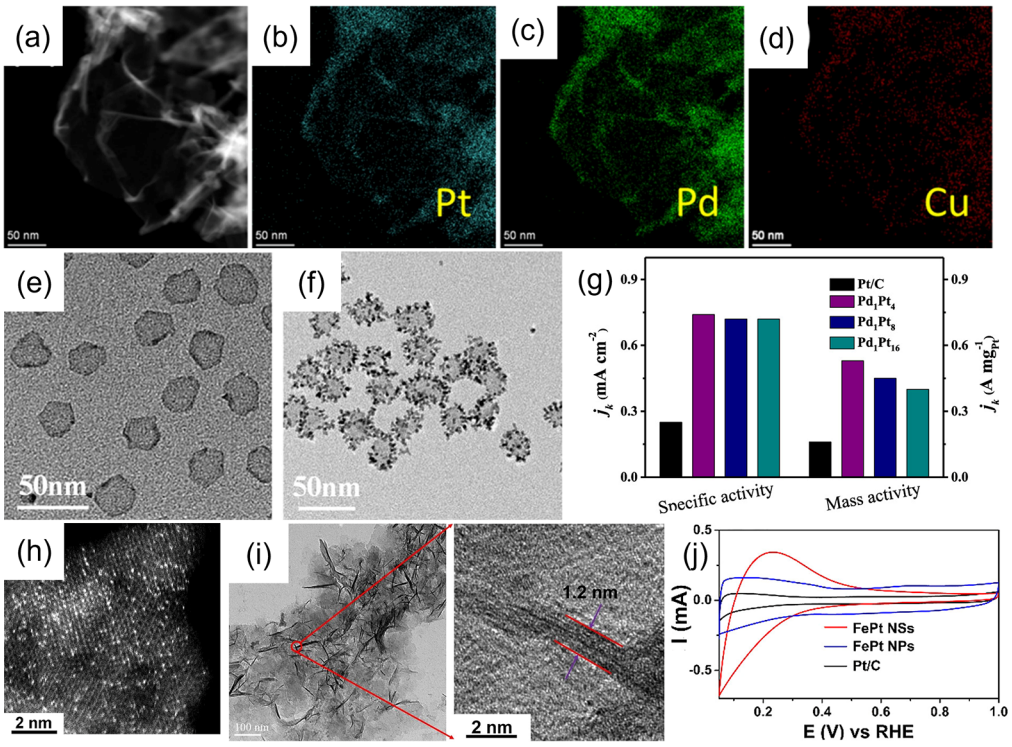


Figure 9. (**a**) HAADF and (**b**–**d**) the corresponding STEM-EDS elemental mapping images of $Pt_{38}Pd_{50}Cu_{12}$ NSs (from ref. [192] with permission); (**e**) TEM image of Pd NSs; (**f**) TEM image of Pd_1Pt_4 DNSs; (**g**) histogram of SAs and MA at 0.9 V vs. RHE (from ref. [193] with permission); (**h**) HAADF-STEM and (**i**) HRTEM images of FePt NS; (**j**) CV curves of FePt NSs, FePt NPs, and Pt/C (from ref. [195] with permission).

3.4. Formic Acid Oxidation Reaction

Direct formic acid fuel cells (DFAFCs), as a new type of clean energy device, have demonstrated significant potential for applications in portable electronic devices, new energy vehicles, and the aerospace industry due to their comprehensive advantages, including high safety, excellent energy-conversion efficiency, outstanding power density, low hazards

emission, and simple structure [196–198]. The core of this fuel cell system lies in the catalytic performance of FAOR at the anode, which operates through a dual pathway competition mechanism: the direct pathway generates carbon dioxide under ideal conditions, while the indirect pathway generates toxic intermediates such as CO [199,200]. Currently, most conventional Pt-group metallic catalysts generate toxic CO intermediates via the indirect pathway, which negatively impacts the catalytic performance [201,202]. To address this challenge, the rapid surface desorption of CO and retention of active sites during the FAOR process have become a key point [203,204]. This has motivated the rational design and controlled preparation of 2D Pt-group metallic electrocatalysts with high FAOR activity and superior selectivity capable of facilitating the direct dehydrogenation pathway [205,206]. For instance, Zhou and co-workers proposed a novel composite catalyst comprising 2D Pd nanosheets decorated with SnO_2 nanoflakes for the FAOR (Figure 10a–c) [207]. Benefiting from the distinct physicochemical properties as well as the strong interactions between the heterointerfaces, the FAOR mass and specific activities of the resultant hybrid catalyst reached 4.96 A mg^{-1}_{Pd} and 216.95 A m^{-2}_{ECSA}, which were 3.76 and 4.26 times higher than those of Pd nanosheets/C, respectively. In situ attenuated total reflection infrared analysis evidenced a promoted formate pathway for the SnO_2-decorated Pd nanosheets, thus affording a suppressed accumulation of CO molecules.

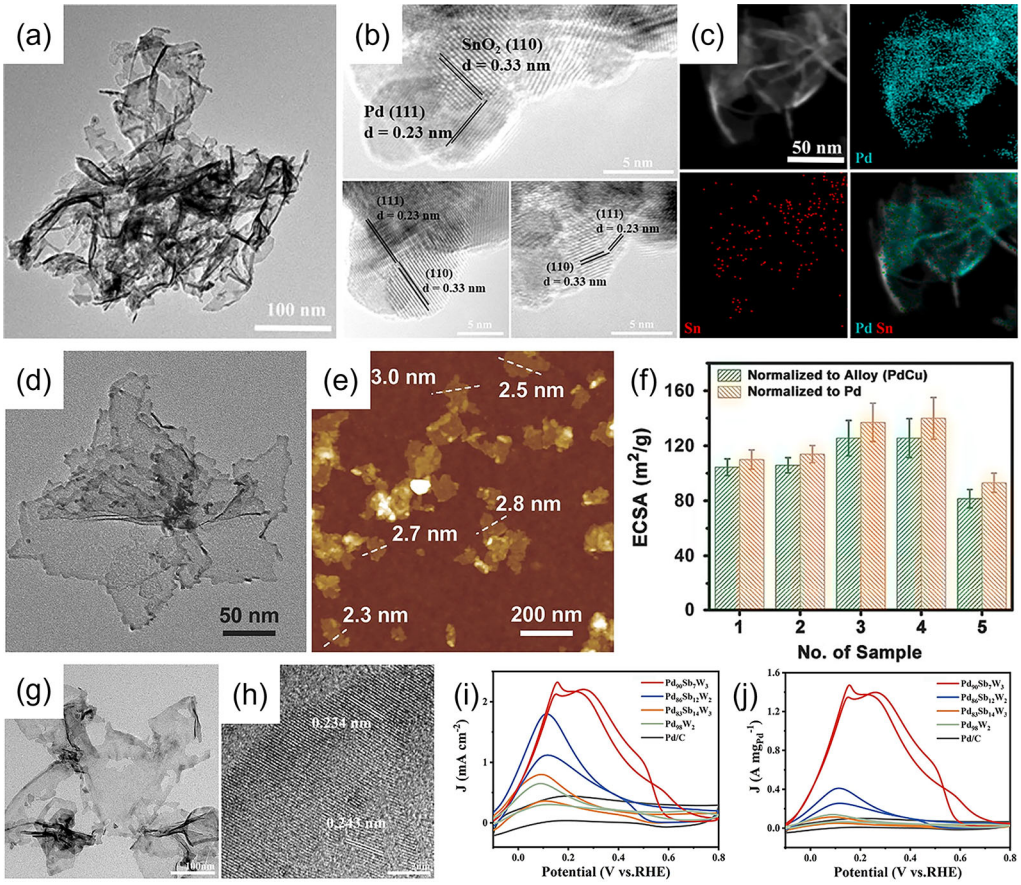


Figure 10. (**a**) Large scale TEM, (**b**) STEM, and (**c**) HRTEM images of Pd@SnO_2-NSs (from ref. [207] with permission); (**d**) TEM and (**e**) AFM images of the synthesized ultrathin PdCu alloy nanosheets; (**f**) ECSAs of various catalysts recorded in 0.5 M H_2SO_4 aqueous solution at a scan rate of 50 mV s^{-1} (from ref. [208] with permission); (**g**) TEM and (**h**) HRTEM images of synthesized $Pd_{90}Sb_7W_3$ nanosheets; (**i**) specific activity and (**j**) mass activity of $Pd_{90}Sb_7W_3$, $Pd_{86}Sb_{12}W_2$, $Pd_{83}Sb_{14}W_3$, $Pd_{98}W_2$ nanosheets, and Pd/C catalysts in 0.5 M H_2SO_4 and 0.5 M HCOOH solution (from ref. [209] with permission).

The precise synthesis of 2D Pd-based bimetallic alloy nanosheets is a feasible strategy to enhance the catalytic efficiency of the FAOR. One important contribution was that Zhang's group innovatively synthesized ultrathin PdCu bimetallic alloy nanosheets with varying Cu/Pd ratios, which were further treated with ethylenediamine (EN) for the FAOR application [208]. As confirmed by the TEM and AFM characterization (Figure 10d,e), the resulting PdCu nanosheets presented an ultrathin nature with a thickness of only about 2.8 nm, which were composed of uniformly distributed Pd and Cu elements. In a 0.5 M H_2SO_4 and 0.25 M HCOOH electrolyte, the EN post-treated PdCu nanosheets exhibited excellent FAOR performance with a maximum ECSA value of 139.8 $m^2\ g_{Pd}{}^{-1}$ and an ultrahigh mass activity of 1655.7 mA $mg_{Pd}{}^{-1}$ (Figure 10f). The dramatically enhanced activity of the EN-treated PdCu alloy nanosheets can be attributed to their ultrathin morphology, ameliorative electronic structure, bimetallic synergistic effects, and removal of inert oleic acid by EN treatment. In another work, Wei et al. successfully synthesized 2D PdSb-based nanosheets by doping the Sb element with a predominant metallic state into the Pd crystal structure (Figure 10g,h) [209]. Notably, metallic Sb operated through the synergistic effects of electronic modification and oxophilic properties, leading to the effective electrooxidation removal of CO species during the FAOR. As shown in Figure 10i,j, the specific and mass activities of the PdSb-based nanosheets with 69% Sb metallic state were significantly higher than those of Pd-based nanosheets and Pd/C catalysts.

3.5. Alcohol Oxidation Reactions

Direct alcohol fuel cells (DAFCs) achieve efficient energy conversion through the electrocatalytic oxidation of alcohol fuels (e.g., methanol, ethanol, ethylene glycol, etc.) [210–212]. Such electrocatalytic processes are environmentally friendly and sustainable, making DAFCs ideal alternatives to traditional heat engines [213–216]. In addition, DAFCs can perform well at various operating temperatures, thus holding huge potential for a wide range of applications [217,218]. Nevertheless, the intrinsic sluggish dynamics for the electrooxidation of alcohol molecules poses a great challenge to the large-scale commercialization of DAFCs [219–221]. For example, there are two competing pathways for the ethanol oxidation reaction (EOR), named "C1" and "C2", which refer to the complete oxidation of ethanol to CO_2 (12-electron transfer, C1 pathway) and partial oxidation to CH_3COOH (4-electron transfer, C2 pathway), respectively [222,223]. Conventional catalyst systems generally exhibit low selectivity of the C1 pathway and high selectivity of the C2 pathway, which largely hinders the efficiency improvement [224,225]. Therefore, the development of efficient, highly-selective anode electrocatalysts that enhance the cleavage of C-C and C-H bonds for the complete oxidation of alcohol molecules is conducive to promoting the widespread application of DAFCs [226–229].

One representative example was published by Chen's group, where hierarchical porous Rh nanosheets were prepared with the help of an emulsion-induced soft template method [230]. Structural characterization revealed that the sample presented a typical lamellar structure, which was constructed from the self-assembly of secondary Rh crystals with rough and porous surfaces (Figure 11a–c). Because of their abundant edge/grain boundary atoms and ultrathin porous structure, the hierarchical porous Rh nanosheets demonstrated enhanced MOR kinetics with a mass activity of 333 A g^{-1} with a relatively low peak potential of 0.63 V, which was 5.8 and 3.3 times higher than those of commercial Pt black and Rh black catalysts, respectively (Figure 11d). In addition, Zhang's group introduced a second metal Ag into Pd crystal lattices and successfully prepared hierarchically interconnected PdAg alloy nanosheets with a thickness of only seven atoms (Figure 11e,f), which were very beneficial to promote both charge transfer and mass transport during the EOR process [231]. As shown in Figure 10g, with a moderate molar ratio of Pd/Ag precur-

sors, the optimized Pd_7Ag_3 nanosheets exhibited a remarkable EOR peak current density of 9365.9 mA mg^{-1}_{Pd}, which was 8.8 times higher than that of reference Pd nanosheets catalyst (1053.7 mA mg^{-1}_{Pd}).

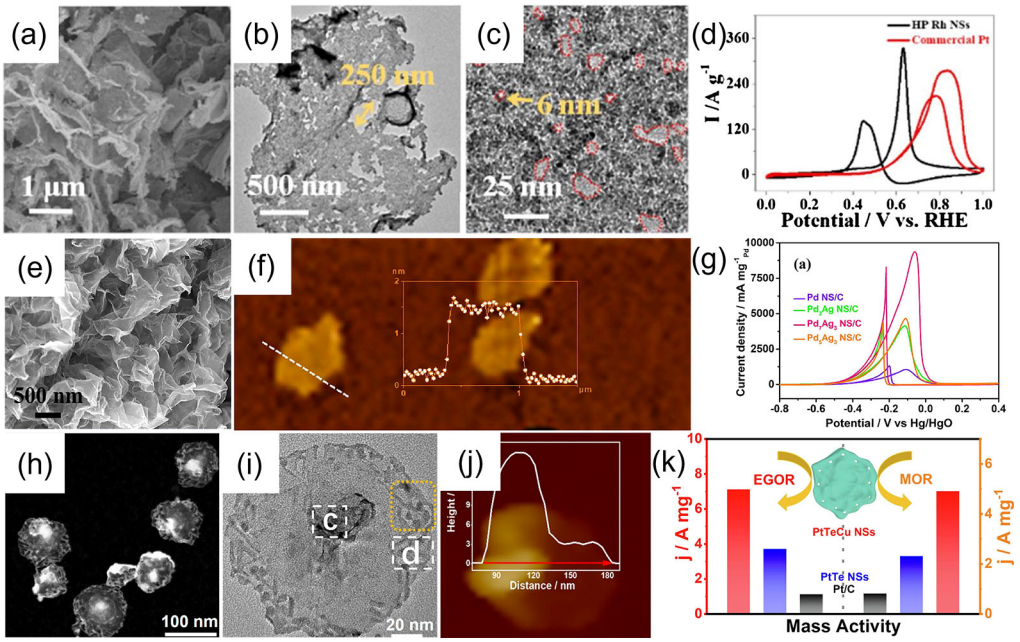


Figure 11. (**a**) SEM and (**b**,**c**) TEM images of HP-Rh NSs; (**d**) mass-normalized CV curves of HP-Rh NSs and commercial Pt black recorded in N_2-saturated 1 M KOH and 0.5 M methanol solution at 50 mV s^{-1} (from ref. [230] with permission); (**e**) SEM, (**f**) AFM images and corresponding height profile of Pd_7Ag_3 NS; (**g**) CV curves of Pd NS/C, Pd_3Ag NS/C, Pd_7Ag_3 NS/C, and Pd_5Ag_3 NS/C in 1.0 M KOH and 1.0 M ethanol electrolyte (from ref. [231], with permission); (**h**) HAADF-STEM, (**i**) TEM, and (**j**) AFM images of PtTeCu NSs; (**k**) mass activity histograms for different catalysts (from ref. [232] with permission).

Precise regulation of the active site distribution through the construction of multi-component configurations has become an important research direction to enhance the catalytic performance of 2D Pt-group metallic materials [233,234]. Dong et al. reported the construction of free-standing ultrathin and highly flexible ternary alloy PtTeCu nanosheets and their use as MOR electrocatalysts (Figure 11h–j) [232]. The nanoporous ultrathin-sheet structure largely facilitated the exposure of Pt active sites, while the introduction of Te and Cu atoms induced an obvious downward shift of the d-band center of Pt and weakened the adsorption energy of the products on the ternary nanosheets. As a result, the PtTeCu nanosheets exhibited a high catalytic performance for the ethylene glycol oxidation reaction (EGOR) and MOR with mass activities of 7.1 and 4.9 A mg^{-1}, which were 6.5 and 6.1 times higher than those of commercial Pt/C, respectively (Figure 11k). Huang's group developed a unique class of Rh/Rh-M nanosheets (M = Co, Mn, Fe, and Ni) by depositing Rh-M nanoparticles on the surface of a 2D Rh nanosheet substrate [235]. Noteworthily, CO could spill over from the Rh sites of ultrathin Rh nanosheets to the M sites of the Rh-M nanoparticles, thus leading to the weakening of CO adsorption on the Rh sites. In regard to the EOR catalysis, it was found that the optimal $Rh_{79}Co_{21}$ nanosheets with the CO spillover effect had a large current density of 485.14 mA $mg_{Rh}{}^{-1}$ and a CO_2 Faraday efficiency of 75.5%, significantly superior to those of bare Rh nanosheets.

4. Conclusions, Challenges, and Perspectives

Over the past few years, 2D Pt-group metallic nanocrystals have attracted considerable and widespread attention because of their significant application value in the field of

clean energy-conversion devices due to their large specific surface area, plentiful unsaturated metal atoms, optimized electronic structure, and unimpeded electron/ion transfer pathways. In this review paper, we have outlined the effective methods for the controllable construction of 2D Pt-group metallic nanocrystals, comprising CO-confined growth methods, self-assembly methods, template methods, in situ growth methods, and so on. Moreover, this review has summarized the latest research progress on the applications of 2D Pt-group metallic nanocrystals as electrocatalysts for a variety of energy-conversion technologies (including HER, OER, ORR, FAOR, and AOR) and highlighted the core relationship between their nanoarchitectural features and electrocatalytic properties.

Although 2D Pt-group metallic electrocatalysts present promising opportunities for addressing critical energy and environmental challenges, their large-scale commercialization remains constrained by several fundamental limitations. Firstly, the thin-sheet Pt-group metallic nanocrystals with high surface free energies easily suffer from longitudinal restacking or re-aggregation during their practical usage, resulting in an obvious decrease in the number of catalytically active sites. Given this, it is recommended to combine 2D Pt-group metallic nanocrystals with high-quality supporting materials (e.g., graphene, MXene, etc.) to construct a 2D/2D heterostructure through a "face-to-face" interfacial interaction, which could largely maintain the catalytic advantages of the separated Pt-group metallic nanosheets. Meanwhile, identifying optimal material combinations from numerous possibilities presents a significant challenge; leveraging artificial intelligence (AI) methods synergistically with high-throughput computing techniques offers an accelerated pathway for discovering and evaluating efficient electrocatalysts based on 2D/2D heterostructures. Secondly, current synthesis processes for the 2D Pt-group metallic electrocatalysts commonly refer to the utilization of various capping agents, including surfactants, templates, and organic ligands, which cannot be effectively removed through conventional purification methods without compromising the structural integrity of the nanosheets. Therefore, it is highly desirable to develop novel surfactant- and template-free synthetic strategies to avoid the excessive use of capping agents and keep the catalytic crystal faces clean. Thirdly, considering the high costs and scarcity of most Pt-group metals, it is suggested to introduce appropriate inexpensive transition metal elements to construct multicomponent metallic systems, especially high-entropy alloys and intermetallic compounds, which could not only reduce the usage amount of Pt-group metals to lower the manufacturing costs but also boost the intrinsic catalytic activity through alloy, strain, lattice distortion, and cocktail effects. Finally, the dynamic surface reconstruction of 2D Pt-group metallic electrocatalysts during diverse energy-conversion reactions obscures the precise identification of actual catalytical active centers, thereby hindering the elucidation of underlying catalytic mechanisms, which requires the exploration and utilization of various in situ characterization techniques combined with advanced theoretical analyses to unveil the structural evolution of active centers and establish robust guidelines for rational catalyst design.

Encouragingly, despite the above research challenges, researchers are still enthusiastic about 2D Pt-group metallic electrocatalysts, with more and more young scholars devoted to this field. With the continuous innovation of nanomaterials as well as breakthroughs in surface/interface regulation technology, the development of this field is expected to catalyze the technological innovation of core devices, such as next-generation PEMFC and metal–air batteries. Such breakthroughs will not only reshape the energy-production and -consumption systems but may also trigger revolutionary changes in green transportation, distributed energy supply, and other application scenarios, thus providing key technological supports for the realization of carbon neutrality.

Author Contributions: Conceptualization, H.H. (Huajie Huang); methodology, Z.C. and H.H. (Huajie Huang); software, Z.C. and Y.W.; validation, Z.C. and Y.W.; formal analysis, Z.C. and H.H. (Haiyan He); investigation, Z.C. and H.H. (Haiyan He); resources, H.H. (Huajie Huang); data curation, Z.C.; writing—original draft preparation, Z.C.; writing—review and editing, H.H. (Huajie Huang); visualization, Z.C.; supervision, H.H. (Huajie Huang); project administration, H.H. (Huajie Huang); funding acquisition, H.H. (Huajie Huang). All authors have read and agreed to the published version of the manuscript.

Funding: This work was supported by the National Natural Science Foundation of China (52472092).

Data Availability Statement: No new data were created or analyzed in this study.

Conflicts of Interest: The authors declare no conflicts of interest.

Abbreviations

The following abbreviations are used in this manuscript:

0D	zero-dimensional
1D	one-dimensional
2D	two-dimensional
3D	three-dimensional
TMDs	transition metal disulfides
h-BN	hexagonal boron nitride
MOFs	metal-organic frameworks
COFs	covalent organic frameworks
HER	hydrogen evolution reaction
OER	oxygen evolution reaction
ORR	oxygen reduction reaction
FAOR	formic acid oxidation reaction
AOR	alcohol oxidation reaction
CO	carbon monoxide
LDHs	layered double hydroxides
RGO	reduced graphene oxide
DFT	density functional theory
PEMWE	polymer electrolyte membrane water electrolyzer
PEMFCs	proton exchange membrane fuel cells
ADT	accelerated durability testing
RRDE	rotating ring disk electrode
DEMS	differential electrochemical mass spectrometry
ECSA	electrochemical active surface area
CV	cyclic voltammetry
LSV	linear sweep voltammetry
MA	mass activity
DFAFCs	direct formic acid fuel cells
EN	ethylenediamine
DAFCs	direct alcohol fuel cells
EGOR	ethylene glycol oxidation reaction
MOR	methanol oxidation reaction

References

1. He, Q.; Sheng, B.; Zhu, K.; Zhou, Y.; Qiao, S.; Wang, Z.; Song, L. Phase Engineering and Synchrotron-Based Study on Two-Dimensional Energy Nanomaterials. *Chem. Rev.* **2023**, *123*, 10750–10807. [CrossRef]
2. Johnson, N.; Liebreich, M.; Kammen, D.M.; Ekins, P.; McKenna, R.; Staffell, I. Realistic Roles for Hydrogen in the Future Energy Transition. *Nat. Rev. Clean Technol.* **2025**, *1*, 351–371. [CrossRef]

3. Qiu, H.; Wen, S.; Fu, Q.; Zhao, X. Oxygen Reduction Reactions of Catalysts with Asymmetric Atomic Structures: Mechanisms, Applications, and Challenges. *Catalysts* **2025**, *15*, 615. [CrossRef]
4. Sun, H.; Xu, X.; Kim, H.; Shao, Z.; Jung, W. Advanced Electrocatalysts with Unusual Active Sites for Electrochemical Water Splitting. *InfoMat* **2023**, *6*, e12494. [CrossRef]
5. Nnabuife, S.G.; Hamzat, A.K.; Whidborne, J.; Kuang, B.; Jenkins, K.W. Integration of Renewable Energy Sources in Tandem with Electrolysis: A Technology Review for Green Hydrogen Production. *Int. J. Hydrogen Energy* **2025**, *107*, 218–240. [CrossRef]
6. He, Q.; Zhou, Y.; Shou, H.; Wang, X.; Zhang, P.; Xu, W.; Qiao, S.; Wu, C.; Liu, H.; Liu, D.; et al. Synergic Reaction Kinetics over Adjacent Ruthenium Sites for Superb Hydrogen Generation in Alkaline Media. *Adv. Mat.* **2022**, *34*, 2110604. [CrossRef]
7. Li, S.; Shu, J.; Ma, S.; Yang, H.; Jin, J.; Zhang, X.; Jin, R. Engineering Three-Dimensional Nitrogen-Doped Carbon Black Embedding Nitrogen-doped Graphene Anchoring Ultrafine Surface-Clean Pd Nanoparticles as Efficient Ethanol Oxidation Electrocatalyst. *Appl. Catal. B Environ.* **2021**, *280*, 119464. [CrossRef]
8. Yang, C.; He, H.; Jiang, Q.; Liu, X.; Shah, S.P.; Huang, H.; Li, W. Pd Nanocrystals Grown on MXene and Reduced Graphene Oxide CO-Constructed Three-Dimensional Nanoarchitectures for Efficient Formic Acid Oxidation Reaction. *Int. J. Hydrogen Energy* **2021**, *46*, 589–598. [CrossRef]
9. Xu, C.; He, H.; Zhu, Y.; Wang, Y.; Hao, L.; Huang, H. Mutual-Coupling 0D/1D/2D Heterostructure of Cobalt Selenide/Carbon Nanotube/MXene for Enhanced Electrocatalytic Hydrogen Evolution. *Int. J. Hydrogen Energy* **2025**, *100*, 1038–1045. [CrossRef]
10. Wang, J.; Kong, H.; Zhang, J.; Hao, Y.; Shao, Z.; Ciucci, F. Carbon-Based Electrocatalysts for Sustainable Energy Applications. *Prog. Mater. Sci.* **2021**, *116*, 100717. [CrossRef]
11. Yao, J.; Huang, W.; Fang, W.; Kuang, M.; Jia, N.; Ren, H.; Liu, D.; Lv, C.; Liu, C.; Xu, J.; et al. Promoting Electrocatalytic Hydrogen Evolution Reaction and Oxygen Evolution Reaction by Fields: Effects of Electric Field, Magnetic Field, Strain, and Light. *Small Methods* **2020**, *4*, 200494. [CrossRef]
12. Yue, L.; Jiang, Q.; Ma, L.; Li, Y.; Yang, L.; Zhang, J.; He, H.; Huang, H. Confined Palladium Nanocrystals within Covalent Organic Framework-Intercalated MXene Nanoarchitectures toward Highly Efficient Methanol Electrooxidation. *Chem. Mater.* **2025**, *37*, 2125–2135. [CrossRef]
13. Wu, X.; Yan, Q.; Wang, H.; Wu, D.; Zhou, H.; Li, H.; Yang, S.; Ma, T.; Zhang, H. Heterostructured Catalytic Materials as Advanced Electrocatalysts: Classification, Synthesis, Characterization, and Application. *Adv. Funct. Mater.* **2024**, *34*, 2404535. [CrossRef]
14. Li, S.; Ma, S.; Zhang, Y.; Zhao, L.; Yang, H.; Jin, R. Metal-Organic Interface Engineering for Coupling Palladium Nanocrystals over Functionalized Graphene as an Advanced Electrocatalyst of Methanol and Ethanol Oxidation. *J. Colloid Interface Sci.* **2021**, *588*, 384–392. [CrossRef]
15. Wang, Y.; Guo, X.; Chen, Z.; Zhang, Y.; He, H.; Huang, H. Palladium Nanocrystals Immobilized on Boron and Nitrogen Codoped Mesoporous Carbon Spheres as Efficient Methanol Oxidation Electrocatalysts. *Colloids Surf. A* **2025**, *705*, 135598. [CrossRef]
16. Wang, H.; Yan, Z.; Cheng, F.; Chen, J. Advances in Noble Metal Electrocatalysts for Acidic Oxygen Evolution Reaction: Construction of Under-Coordinated Active Sites. *Adv. Sci.* **2024**, *11*, 2401652. [CrossRef]
17. Gao, G.; Zhao, G.; Zhu, G.; Sun, B.; Sun, Z.; Li, S.; Lan, Y.-Q. Recent Advancements in Noble-Metal Electrocatalysts for Alkaline Hydrogen Evolution Reaction. *Chin. Chem. Lett.* **2025**, *36*, 109557. [CrossRef]
18. Xiong, J.; Zhang, Q.; He, H.; Huang, H. Ultrasmall Rh-Decorated Porous Heterostructures Stereoassembled from MXene and Graphene for Efficient Methanol Electrooxidation. *Int. J. Hydrogen Energy* **2024**, *92*, 535–543. [CrossRef]
19. Wang, Y.; Chen, Z.; Zhang, C.; Yang, L.; Jiang, Q.; Zhang, J.; He, H.; Huang, H. Mesoporous Hollow Carbon Sphere-Embedded MXene Architectures Decorated with Ultrafine Rh Nanocrystals toward Methanol Electrooxidation. *Inorg. Chem.* **2024**, *63*, 16888–16896. [CrossRef]
20. Huang, C.; Wang, F.; Chen, X.; Li, J.; Shao, M.; Wei, Z. Innovative Strategies for Designing and Constructing Efficient Fuel Cell Electrocatalysts. *Chem. Commun.* **2025**, *61*, 2658–2683. [CrossRef]
21. Shu, J.; Li, R.; Lian, Z.; Zhang, W.; Jin, R.; Yang, H.; Li, S. In-Situ Oxidation of Palladium–Iridium Nanoalloy Anchored on Nitrogen-Doped Graphene as an Efficient Catalyst for Methanol Electrooxidation. *J. Colloid Interface Sci.* **2022**, *605*, 44–53. [CrossRef]
22. Zhang, Q.; Deng, Z.; He, H.; Ying, G.; Huang, H. Immobilizing Ultrafine PtRu Alloy Nanoparticles onto 3D Interconnected MXene-Graphene Frameworks for Highly Efficient Methanol Oxidation. *Ceram. Int.* **2024**, *50*, 16443–16451. [CrossRef]
23. Huang, H.; Wei, Y.; Yang, Y.; Yan, M.; He, H.; Jiang, Q.; Yang, X.; Zhu, J. Controllable Synthesis of Grain Boundary-Enriched Pt Nanoworms Decorated on Graphitic Carbon Nanosheets for Ultrahigh Methanol Oxidation Catalytic Activity. *J. Energy Chem.* **2021**, *57*, 601–609. [CrossRef]
24. Meng, W.; He, H.; Yang, L.; Jiang, Q.; Yuliarto, B.; Yamauchi, Y.; Xu, X.; Huang, H. 1D-2D Hybridization: Nanoarchitectonics for Grain Boundary-Rich Platinum Nanowires Coupled with MXene Nanosheets as Efficient Methanol Oxidation Electrocatalysts. *Chem. Eng. J.* **2022**, *450*, 137932. [CrossRef]

25. Zhang, Q.; Yan, M.-M.; Du, W.-F.; Yin, C.-Y.; Zhang, J.; Yang, L.; Kang, Y.-Q.; He, H.-Y.; Huang, H.-J. Spatial Construction of Ultrasmall Pt-Decorated 3D Spinel Oxide-Modified N-Doped Graphene Nanoarchitectures as High-Efficiency Methanol Oxidation Electrocatalysts. *Rare Met.* **2023**, *43*, 186–197. [CrossRef]
26. Hu, X.; Yang, B.; Ke, S.; Liu, Y.; Fang, M.; Huang, Z.; Min, X. Review and Perspectives of Carbon-Supported Platinum-Based Catalysts for Proton Exchange Membrane Fuel Cells. *Energy Fuels* **2023**, *37*, 11532–11566. [CrossRef]
27. Liu, D.; Li, X.; Chen, S.; Yan, H.; Wang, C.; Wu, C.; Haleem, Y.A.; Duan, S.; Lu, J.; Ge, B.; et al. Atomically Dispersed Platinum Supported on Curved Carbon Supports for Efficient Electrocatalytic Hydrogen Evolution. *Nat. Energy* **2019**, *4*, 512–518. [CrossRef]
28. Wang, W.; Lv, F.; Lei, B.; Wan, S.; Luo, M.; Guo, S. Tuning Nanowires and Nanotubes for Efficient Fuel-Cell Electrocatalysis. *Adv. Mater.* **2016**, *28*, 10117–10141. [CrossRef]
29. Huang, H.; Zhang, Q.; Meng, W.; Yang, C.; Jiang, Q.; Zhang, C.; He, H.; Ying, G. Grain Boundary-Enriched Wavy Pd Nanowires Intertwined with MXene Nanosheets toward Formic Acid and Methanol Electrooxidation. *Inorg. Chem.* **2025**, *64*, 7690–7697. [CrossRef]
30. Shen, B.; Wei, Y.; Sun, P.; He, H.; Ying, G.; Huang, H. Immobilizing Ultrasmall Pt nanocrystals on 3D Interweaving BCN Nanosheet-Graphene Networks Enables Efficient Methanol Oxidation Reaction. *Dalton Trans.* **2023**, *52*, 13644–13652. [CrossRef]
31. Zhu, Z.; Qin, J.; Yang, Q.; He, H.; Yang, L.; Huang, H.; Ying, G. Interconnected Pd Nanowire Networks Stereoassembled on Biomass-Derived Porous Carbon Skeletons as Bifunctional Electrocatalysts for Efficient Methanol and Formic Acid Oxidation. *ACS Sustain. Chem. Eng.* **2024**, *12*, 10615–10623. [CrossRef]
32. Xiao, D.; Jiang, Q.; Xu, C.; Yang, C.; Yang, L.; He, H.; Huang, H. Interfacial Engineering of Worm-Shaped Palladium Nanocrystals Anchored on Polyelectrolyte-Modified MXene Nanosheets for Highly Efficient Methanol Oxidation. *J. Colloid Interface Sci.* **2022**, *616*, 781–790. [CrossRef]
33. Wang, Y.; Yang, X.; Zhang, Y.; Zhang, C.; Yang, L.; Jiang, Q.; He, H.; Ying, G.; Huang, H. Carbon Nanotube-Bridged MXene Nanoarchitectures Decorated with Ultrasmall Rh Nanoparticles for Efficient Methanol Oxidation. *Mater. Today Energy* **2024**, *40*, 101495. [CrossRef]
34. Chen, T.; Kong, X.; Liu, Q. RuCu Nanorod Arrays Synergistically Promote Efficient Water-Splitting. *Catalysts* **2025**, *15*, 98. [CrossRef]
35. Huang, H.; Guo, X.; Zhang, C.; Yang, L.; Jiang, Q.; He, H.; Amin, M.A.; Alshahrani, W.A.; Zhang, J.; Xu, X.; et al. Advancements in Noble Metal-Decorated Porous Carbon Nanoarchitectures: Key Catalysts for Direct Liquid Fuel Cells. *ACS Nano* **2024**, *18*, 10341–10373. [CrossRef]
36. Chen, T.; Li, Y.; Li, L.; Zhao, Y.; Shi, S.; Jiang, R.; Ma, H. Cu Modified Pt Nanoflowers with Preferential (100) Surfaces for Selective Electroreduction of Nitrate. *Catalysts* **2019**, *9*, 536. [CrossRef]
37. Yang, S.; Chen, Y.; Jiang, C. Strain Engineering of Two-Dimensional Materials: Methods, Properties, and Applications. *InfoMat* **2021**, *3*, 397–420. [CrossRef]
38. Zhao, Y.; Niu, S.; Xi, B.; Du, Z.; Yu, T.; Wan, T.; Lei, C.; Lyu, S. Recent Developments in Two-Dimensional Carbon-Based Nanomaterials for Electrochemical Water Oxidation: A Mini Review. *Catalysts* **2024**, *14*, 221. [CrossRef]
39. Wang, J.; Du, C.F.; Xue, Y.; Tan, X.; Kang, J.; Gao, Y.; Yu, H.; Yan, Q. MXenes as a Versatile Platform for Reactive Surface Modification and Superior Sodium-Ion Storages. *Exploration* **2021**, *1*, 20210024. [CrossRef]
40. Liu, L.; Lian, H.; Deng, H.; Zhang, W. Mxene-Supported Ni–Co Bimetallic MOF 2D Lamellar Membrane for Enhanced Electrochemical Oxygen Reactions and Li–O_2 Battery. *Sci. Rep.* **2025**, *15*, 13995. [CrossRef]
41. Tian, Y.; An, Y.; Feng, J.; Qian, Y. Mxenes and their Derivatives for Advanced Aqueous Rechargeable Batteries. *Mater. Today* **2022**, *52*, 225–249. [CrossRef]
42. Zhao, J.; Li, T.; Yue, Y.; Li, X.; Xie, Z.; Zhang, H.; Tian, X. Advancements in Employing Two-Dimensional Nanomaterials for Enhancing Skin Wound Healing: A Review of Current Practice. *J. Nanobiotechnol.* **2024**, *22*, 520. [CrossRef]
43. Yang, C.; Huang, H.; He, H.; Yang, L.; Jiang, Q.; Li, W. Recent Advances in Mxene-Based Nanoarchitectures as Electrode Materials for Future Energy Generation and Conversion Applications. *Coord. Chem. Rev.* **2021**, *435*, 213806. [CrossRef]
44. Xu, H.; Shang, H.; Wang, C.; Du, Y. Recent Progress of Ultrathin 2D Pd-Based Nanomaterials for Fuel Cell Electrocatalysis. *Small* **2021**, *17*, 2005092. [CrossRef]
45. Tian, H.; Yu, Y.; Wang, Q.; Li, J.; Rao, P.; Li, R.; Du, Y.; Jia, C.; Luo, J.; Deng, P.; et al. Recent Advances in Two-Dimensional Pt Based Electrocatalysts for Methanol Oxidation Reaction. *Int. J. Hydrogen Energy* **2021**, *46*, 31202–31215. [CrossRef]
46. Tian, J.; Song, Y.; Hao, X.; Wang, X.; Shen, Y.; Liu, P.; Wei, Z.; Liao, T.; Jiang, L.; Guo, J.; et al. Greatly Enhanced Oxygen Reduction Reaction in Anion Exchange Membrane Fuel Cell and Zn-Air Battery via Hole Inner Edge Reconstruction of 2D Pd Nanomesh. *Adv. Mater.* **2024**, *37*, 2412051. [CrossRef]
47. Gu, X.; Wang, D.; Zhang, N.; Zhang, Y.; Ye, C.; Du, Y. Solvothermal Synthesis of PdCu Nanorings with High Catalytic Performance for Alcohol Electrooxidation. *J. Colloid Interface Sci.* **2025**, *677*, 750–757. [CrossRef]

48. Gu, B.S.; Dutta, S.; Hong, Y.R.; Ngome Okello, O.F.; Im, H.; Ahn, S.; Choi, S.Y.; Woo Han, J.; Ryu, S.; Lee, I.S. Harmonious Heterointerfaces Formed on 2D-Pt Nanodendrites by Facet-Respective Stepwise Metal Deposition for Enhanced Hydrogen Evolution Reaction. *Angew. Chem. Int. Ed.* **2023**, *62*, e202307816. [CrossRef]
49. Zhu, E.; Yan, X.; Wang, S.; Xu, M.; Wang, C.; Liu, H.; Huang, J.; Xue, W.; Cai, J.; Heinz, H.; et al. Peptide-Assisted 2-D Assembly toward Free-Floating Ultrathin Platinum Nanoplates as Effective Electrocatalysts. *Nano Lett.* **2019**, *19*, 3730–3736. [CrossRef]
50. Tian, J.; Rao, Y.; Shi, W.; Yang, J.; Ning, W.; Li, H.; Yao, Y.; Zhou, H.; Guo, S. Sabatier Relations in Electrocatalysts Based on High-entropy Alloys with Wide-distributed d-band Centers for Li-O_2 Batteries. *Angew. Chem. Int. Ed.* **2023**, *62*, e202310894. [CrossRef]
51. Chen, Z.; Liu, Z.; Xu, X. Dynamic Evolution of the Active Center Driven by Hemilabile Coordination in Cu/CeO_2 Single-Atom Catalyst. *Nat. Commun.* **2023**, *14*, 2512. [CrossRef]
52. Hu, S.; Li, W.-X. Sabatier Principle of Metal-Support Interaction for Design of Ultrastable Metal Nanocatalysts. *Science* **2021**, *374*, 1360–1365. [CrossRef]
53. Chen, Z.W.; Li, J.; Ou, P.; Huang, J.E.; Wen, Z.; Chen, L.; Yao, X.; Cai, G.; Yang, C.C.; Singh, C.V.; et al. Unusual Sabatier Principle on High Entropy Alloy Catalysts for Hydrogen Evolution Reactions. *Nat. Commun.* **2024**, *15*, 359. [CrossRef]
54. Yang, C.; Wang, T.; Li, C.; He, H.; Liu, D.; Huang, H. PdMo Bimetallene Coupled with MXene Nanosheets as Efficient Bifunctional Electrocatalysts for Formic Acid and Methanol Oxidation Reactions. *ACS Appl. Mater. Interfaces* **2023**, *15*, 49195–49203. [CrossRef]
55. Wei, J.; Song, Y.; Gan, M.; An, G.; Shen, Y.; Zhao, X.; Zhang, Y.; Liu, P.; Xu, B.; Guo, J. A Heterostructure Coupling of Ru Nanosheets and NiCo LDH for Hydrazine-Assisted Overall Seawater Splitting. *Sustain. Mater. Technol.* **2025**, *44*, e01413. [CrossRef]
56. Cui, Z.; Bai, X. Ultrasonic-Assisted Synthesis of Two Dimensional Coral-Like Pd Nanosheets Supported on Reduced Graphene Oxide for Enhanced Electrocatalytic Performance. *Ultrason. Sonochem.* **2021**, *70*, 105309. [CrossRef]
57. He, H.; Lan, Y.; Qin, J.; Jiang, Q.; Yang, L.; Zhang, J.; Huang, H. Three-Dimensional Porous Rhodium–Copper Alloy Nanoflowers Stereoassembled on $Ti_3C_2T_x$ MXene as Highly-Efficient Methanol Oxidation Electrocatalysts. *Inorg. Chem. Front.* **2024**, *11*, 8564–8574. [CrossRef]
58. Zhao, F.; Nie, S.; Wu, L.; Yuan, Q.; Wang, X. Porous, Ultrathin PtAgBiTe Nanosheets for Direct Hydrazine Hydrate Fuel Cell Devices. *Adv. Mater.* **2023**, *35*, 2303672. [CrossRef]
59. Li, L.; Bu, L.; Huang, B.; Wang, P.; Shen, C.; Bai, S.; Chan, T.S.; Shao, Q.; Hu, Z.; Huang, X. Compensating Electronic Effect Enables Fast Site-to-Site Electron Transfer over Ultrathin RuMn Nanosheet Branches toward Highly Electroactive and Stable Water Splitting. *Adv. Mater.* **2021**, *33*, 2105308. [CrossRef]
60. Qin, J.; Huang, H.; Xie, Y.; Pan, S.; Chen, Y.; Yang, L.; Jiang, Q.; He, H. MXene Supported Rhodium Nanocrystals for Efficient Electrocatalysts towards Methanol Oxidation. *Ceram. Int.* **2022**, *48*, 15327–15333. [CrossRef]
61. Yang, C.; Jiang, Q.; Liu, H.; Yang, L.; He, H.; Huang, H.; Li, W. Pt-on-Pd Bimetallic Nanodendrites Stereoassembled on MXene Nanosheets for Use as High-Efficiency Electrocatalysts toward the Methanol Oxidation Reaction. *J. Mater. Chem. A* **2021**, *9*, 15432–15440. [CrossRef]
62. Yang, C.; Jiang, Q.; Huang, H.; He, H.; Yang, L.; Li, W. Polyelectrolyte-Induced Stereoassembly of Grain Boundary-Enriched Platinum Nanoworms on $Ti_3C_2T_x$ MXene Nanosheets for Efficient Methanol Oxidation. *ACS Appl. Mater. Interfaces* **2020**, *12*, 23822–23830. [CrossRef]
63. Huang, H.; Wei, Y.; Shen, B.; Zhang, Y.; He, H.; Jiang, Q.; Yang, L.; Nanjundan, A.K.; Na, J.; Xu, X.; et al. Synthesis of Multiple-Twinned Pd Nanoparticles Anchored on Graphitic Carbon Nanosheets for Use as Highly-Active Multifunctional Electrocatalyst in Formic Acid and Methanol Oxidation Reactions. *Adv. Mater. Interfaces* **2020**, *7*, 2000142. [CrossRef]
64. Shi, L.; Wang, Q.; Ren, Q.; Yang, Q.; Zhao, D.; Feng, Y.; Chen, H.; Wang, Y. Facile Synthesis of Pd and PdPtNi Trimetallic Nanosheets as Enhanced Oxygen Reduction Electrocatalysts. *Small* **2021**, *18*, 2103665. [CrossRef]
65. Wang, J.; Zhang, W.; Dong, Z.; Zhang, N.; Zhang, Q.; Xie, C.; Wu, Z.; Xu, G.-R.; Wang, L. One-Step CO Assisted Synthesis of Hierarchical Porous PdRuCu Nanosheets as Advanced Bifunctional Catalysts for Hydrogen Evolution and Glycerol Oxidation. *Int. J. Hydrogen Energy* **2022**, *47*, 33319–33328. [CrossRef]
66. Luo, M.; Zhao, Z.; Zhang, Y.; Sun, Y.; Xing, Y.; Lv, F.; Yang, Y.; Zhang, X.; Hwang, S.; Qin, Y.; et al. PdMo Bimetallene for Oxygen Reduction Catalysis. *Nature* **2019**, *574*, 81–85. [CrossRef]
67. Zhang, L.Y.; Ouyang, Y.; Wang, S.; Wu, D.; Jiang, M.; Wang, F.; Yuan, W.; Li, C.M. Perforated Pd Nanosheets with Crystalline/Amorphous Heterostructures as a Highly Active Robust Catalyst toward Formic Acid Oxidation. *Small* **2019**, *15*, 1904245. [CrossRef]
68. Zhu, W.; Zhang, L.; Yang, P.; Hu, C.; Luo, Z.; Chang, X.; Zhao, Z.J.; Gong, J. Low-Coordinated Edge Sites on Ultrathin Palladium Nanosheets Boost Carbon Dioxide Electroreduction Performance. *Angew. Chem. Int. Ed.* **2018**, *57*, 11544–11548. [CrossRef]
69. Cheng, Z.; Huang, B.; Pi, Y.; Li, L.; Shao, Q.; Huang, X. Partially Hydroxylated Ultrathin Iridium Nanosheets as Efficient Electrocatalysts for Water Splitting. *Natl. Sci. Rev.* **2020**, *7*, 1340–1348. [CrossRef]
70. Wang, H.; Wang, W.; Mao, Q.; Yu, H.; Deng, K.; Xu, Y.; Li, X.; Wang, Z.; Wang, L. Tensile Strained PdNi Bimetallene for Energy-Efficient Hydrogen Production Integrated with Formate Oxidation. *Chem. Eng. J.* **2022**, *450*, 137995. [CrossRef]

71. Huang, X.; Tang, S.; Mu, X.; Dai, Y.; Chen, G.; Zhou, Z.; Ruan, F.; Yang, Z.; Zheng, N. Freestanding Palladium Nanosheets with Plasmonic and Catalytic Properties. *Nat. Nanotechnol.* **2010**, *6*, 28–32. [CrossRef]
72. Zhao, Y.; Tan, X.; Yang, W.; Jia, C.; Chen, X.; Ren, W.; Smith, S.C.; Zhao, C. Surface Reconstruction of Ultrathin Palladium Nanosheets During Electrocatalytic CO_2 Reduction. *Angew. Chem. Int. Ed.* **2020**, *59*, 21493–21498. [CrossRef]
73. Zhao, L.; Xu, C.; Su, H.; Liang, J.; Lin, S.; Gu, L.; Wang, X.; Chen, M.; Zheng, N. Single-Crystalline Rhodium Nanosheets with Atomic Thickness. *Adv. Sci.* **2015**, *2*, 1500100. [CrossRef]
74. Yang, X.; Ouyang, B.; Zhao, L.; Shen, Q.; Chen, G.; Sun, Y.; Li, C.; Xu, K. Ultrathin Rh Nanosheets with Rich Grain Boundaries for Efficient Hydrogen Oxidation Electrocatalysis. *J. Am. Chem. Soc.* **2023**, *145*, 27010–27021. [CrossRef]
75. Ando, S.; Yamamoto, E.; Kobayashi, M.; Kumatani, A.; Osada, M. Facile Synthesis of Pd Nanosheets and Implications for Superior Catalytic Activity. *ACS Nano* **2023**, *18*, 461–469. [CrossRef]
76. Wang, W.; Zhang, X.; Zhang, Y.; Chen, X.; Ye, J.; Chen, J.; Lyu, Z.; Chen, X.; Kuang, Q.; Xie, S.; et al. Edge Enrichment of Ultrathin 2D PdPtCu Trimetallic Nanostructures Effectuates Top-Ranked Ethanol Electrooxidation. *Nano Lett.* **2020**, *20*, 5458–5464. [CrossRef]
77. Zhang, J.; Liu, X.; Ji, Y.; Liu, X.; Su, D.; Zhuang, Z.; Chang, Y.-C.; Pao, C.-W.; Shao, Q.; Hu, Z.; et al. Atomic-Thick Metastable Phase RhMo Nanosheets for Hydrogen Oxidation Catalysis. *Nat. Commun.* **2023**, *14*, 1761. [CrossRef]
78. Wang, Z.; Tian, P.; Zhang, H.; Deng, K.; Yu, H.; Xu, Y.; Li, X.; Wang, H.; Wang, L. PdCu Bimetallene for Enhanced Oxygen Reduction Electrocatalysis. *Inorg. Chem.* **2023**, *62*, 5622–5629. [CrossRef]
79. Wang, D.; Zhang, Y.; Li, J.; Zhang, N.; Wu, Z.; Du, Y. Rapid Synthesis of PdCu Nanosheets with Enhanced Electrocatalytic Activity toward Polyalcohol Oxidation Reaction. *Int. J. Hydrogen Energy* **2024**, *74*, 193–200. [CrossRef]
80. Chu, X.; Wang, X.; Wei, R.; Yan, M.; Wei, X.; Zhang, X.; Zhu, Z.; Wang, Y.; Wang, L.; Yin, S. Defect-Rich PdCo Bimetallene Constructed by a Self-Reduction Strategy for Enhanced Ethanol Oxidation Reaction. *Mater. Today Phys.* **2024**, *43*, 101416. [CrossRef]
81. Wang, D.; Zhang, Y.; Zhang, K.; Wang, X.; Wang, C.; Li, Z.; Gao, F.; Du, Y. Rapid Synthesis of Palladium-Platinum-Nickel Ultrathin Porous Nanosheets with High Catalytic Performance for Alcohol Electrooxidation. *J. Colloid Interface Sci.* **2023**, *650*, 350–357. [CrossRef]
82. Ao, Y.; Ling, X.; Zheng, J.; Han, M.; Xu, D. Effective PdPtMoCrCoNi Alloy Nanosheets Boost Electrocatalytic Activity and Stability for Ethylene Glycol Oxidation. *Surf. Interfaces.* **2024**, *45*, 103928. [CrossRef]
83. Li, H.; Zeng, R.; Feng, X.; Wang, H.; Xu, W.; Lu, X.; Xie, Z.; Abruña, H.D. Oxidative Stability Matters: A Case Study of Palladium Hydride Nanosheets for Alkaline Fuel Cells. *J. Am. Chem. Soc.* **2022**, *144*, 8106–8114. [CrossRef]
84. Zhao, Y.; Bai, J.; Wu, X.-R.; Chen, P.; Jin, P.-J.; Yao, H.-C.; Chen, Y. Atomically Ultrathin RhCo Alloy Nanosheet Aggregates for Efficient Water Electrolysis in Broad Ph Range. *J. Mater. Chem. A* **2019**, *7*, 16437–16446. [CrossRef]
85. Gao, C.; Sun, H.; Du, J. Unusual Endotaxy Growth of Hexagonal Nanosheets by the Self-Assembly of a Homopolymer. *Angew. Chem. Int. Ed.* **2025**, *64*, 2420079. [CrossRef]
86. Ariga, K.; Nishikawa, M.; Mori, T.; Takeya, J.; Shrestha, L.K.; Hill, J.P. Self-Assembly as a Key Player for Materials Nanoarchitectonics. *Sci. Technol. Adv. Mater.* **2019**, *20*, 51–95. [CrossRef]
87. Cai, R.; Yang, D.; Lin, K.-T.; Lyu, Y.; Zhu, B.; He, Z.; Zhang, L.; Kitamura, Y.; Qiu, L.; Chen, X.; et al. Generalized Preparation of Two-Dimensional Quasi-nanosheets via Self-assembly of Nanoparticles. *J. Am. Chem. Soc.* **2019**, *141*, 1725–1734. [CrossRef]
88. Saleem, F.; Xu, B.; Ni, B.; Liu, H.; Nosheen, F.; Li, H.; Wang, X. Atomically Thick Pt-Cu Nanosheets: Self-Assembled Sandwich and Nanoring-Like Structures. *Adv. Mater.* **2015**, *27*, 2013–2018. [CrossRef]
89. Li, Z.; Li, H.; Li, M.; Hu, J.; Liu, Y.; Sun, D.; Fu, G.; Tang, Y. Iminodiacetonitrile Induce-Synthesis of Two-Dimensional PdNi/Ni@Carbon Nanosheets with Uniform Dispersion and Strong Interface Bonding as an Effective Bifunctional Eletrocatalyst in Air-Cathode. *Energy Storage Mater.* **2021**, *42*, 118–128. [CrossRef]
90. Saravani, H.; Farsadrooh, M.; Mollashahi, M.S.; Hajnajafi, M.; Douk, A.S. Two-Dimensional Engineering of Pd Nanosheets as Advanced Electrocatalysts toward Formic Acid Oxidation. *Int. J. Hydrogen Energy* **2020**, *45*, 21232–21240. [CrossRef]
91. Zu, L.; Qian, X.; Zhao, S.; Liang, Q.; Chen, Y.E.; Liu, M.; Su, B.-J.; Wu, K.-H.; Qu, L.; Duan, L.; et al. Self-Assembly of Ir-Based Nanosheets with Ordered Interlayer Space for Enhanced Electrocatalytic Water Oxidation. *J. Am. Chem. Soc.* **2022**, *144*, 2208–2217. [CrossRef]
92. Fu, L.; Liu, K.; Zhen, C.; Zhu, Y.; Lyu, Z.; Du, G.; Xie, S. Lamellar-Assembled PdNi Super-Nanosheets as Effective Oxygen Redox Dual-Electrocatalysts for Rechargeable Zn-Air Batteries. *Nano Res.* **2022**, *16*, 2163–2169. [CrossRef]
93. Qiu, X.; Zhang, H.; Wu, P.; Zhang, F.; Wei, S.; Sun, D.; Xu, L.; Tang, Y. One-Pot Synthesis of Freestanding Porous Palladium Nanosheets as Highly Efficient Electrocatalysts for Formic Acid Oxidation. *Adv. Funct. Mater.* **2016**, *27*, 1603852. [CrossRef]
94. Jiang, N.; Niu, X.; Liu, D.; Zhang, K.; Guo, Z.; Qin, Y.; Zhao, W.; Zhang, X.; Wang, Q. Constructing Pt/Hierarchical HY Bifunctional Catalysts for Selective Hydroisomerization of Phenanthrene to Alkyl-Adamantanes. *Catalysts* **2025**, *15*, 413. [CrossRef]
95. Shin, H.J.; Ryoo, R.; Liu, Z.; Terasaki, O. Template Synthesis of Asymmetrically Mesostructured Platinum Networks. *J. Am. Chem. Soc.* **2001**, *123*, 1246–1247. [CrossRef]

96. Burpo, F.J.; Nagelli, E.A.; Losch, A.R.; Bui, J.K.; Forcherio, G.T.; Baker, D.R.; McClure, J.P.; Bartolucci, S.F.; Chu, D.D. Salt-Templated Platinum-Copper Porous Macrobeams for Ethanol Oxidation. *Catalysts* **2019**, *9*, 662. [CrossRef]
97. Liu, J.; Liu, Z.; Wang, H.; Liu, B.; Zhao, N.; Zhong, C.; Hu, W. Designing Nanoporous Coral-Like Pt Nanowires Architecture for Methanol and Ammonia Oxidation Reactions. *Adv. Funct. Mater.* **2021**, *32*, 2110702. [CrossRef]
98. Chen, Y.-Z.; Zhou, M.; Huang, Y.-F.; Ma, Y.-Y.; Yan, L.-Y.; Zhou, X.-W.; Ma, X.-Z.; Zhao, X.-L.; Chen, C.; Bai, J.; et al. Enhanced Ethanol Oxidation over Pd Nanoparticles Supported Porous Graphene-Doped MXene Using Polystyrene Particles as Sacrificial Templates. *Rare Met.* **2022**, *41*, 3170–3179. [CrossRef]
99. Li, Y.; Liu, Y.; Li, J.; Xiong, D.; Chen, X.; Liu, M.; Zhong, Z.; Malgras, V.; Bando, Y.; Yamauchi, Y.; et al. A Centimeter Scale Self-Standing Two-Dimensional Ultra-Thin Mesoporous Platinum Nanosheet. *Mater. Horiz.* **2020**, *7*, 489–494. [CrossRef]
100. Xu, D.; Liu, X.; Lv, H.; Liu, Y.; Zhao, S.; Han, M.; Bao, J.; He, J.; Liu, B. Ultrathin Palladium Nanosheets with Selectively Controlled Surface Facets. *Chem. Sci.* **2018**, *9*, 4451–4455. [CrossRef]
101. Yamamoto, E.; Suzuki, A.; Kobayashi, M.; Osada, M. Tailored Synthesis of Molecularly Thin Platinum Nanosheets Using Designed 2D Surfactant Solids. *Nanoscale* **2022**, *14*, 11561–11567. [CrossRef]
102. Teng, Z.; Li, M.; Li, Z.; Liu, Z.; Fu, G.; Tang, Y. Facile Synthesis of Channel-Rich Ultrathin Palladium-Silver Nanosheets for Highly Efficient Formic Acid Electrooxidation. *Mater. Today Energy* **2021**, *19*, 100596. [CrossRef]
103. Li, H.; Li, L.; Yang, W.; Yang, J.; Wang, S.; Zhang, H.; Cui, P.; Yin, S.; Wang, Y.; Qi, J. Binary Nonmetal Boron and Phosphorus CO-Doping into PdRh Nanosheets Boosts Electro-Upgrading Polyethylene Terephthalate. *Chem. Eng. J.* **2024**, *490*, 151696. [CrossRef]
104. Jang, S.W.; Dutta, S.; Kumar, A.; Hong, Y.-R.; Kang, H.; Lee, S.; Ryu, S.; Choi, W.; Lee, I.S. Holey Pt Nanosheets on NiFe-Hydroxide Laminates: Synergistically Enhanced Electrocatalytic 2D Interface toward Hydrogen Evolution Reaction. *ACS Nano* **2020**, *14*, 10578–10588. [CrossRef]
105. Gu, K.; Pan, X.; Wang, W.; Ma, J.; Sun, Y.; Yang, H.; Shen, H.; Huang, Z.; Liu, H. In Situ Growth of Pd Nanosheets on g-C_3N_4 Nanosheets with Well-Contacted Interface and Enhanced Catalytic Performance for 4-Nitrophenol Reduction. *Small* **2018**, *14*, 1801812. [CrossRef]
106. Chen, M.-T.; Zhang, R.-L.; Feng, J.-J.; Mei, L.-P.; Jiao, Y.; Zhang, L.; Wang, A.-J. A Facile One-Pot Room-Temperature Growth of Self-Supported Ultrathin Rhodium-Iridium Nanosheets as High-Efficiency Electrocatalysts for Hydrogen Evolution Reaction. *J. Colloid Interface Sci.* **2022**, *606*, 1707–1714. [CrossRef]
107. Bao, X.; Gong, Y.; Zheng, X.; Chen, J.; Mao, S.; Wang, Y. Highly Performed Platinum Nanosheets Synthesized under in Situ Reaction Conditions for Hydrogen Generation. *J. Energy Chem.* **2020**, *51*, 272–279. [CrossRef]
108. Yang, S.; Qiu, P.; Yang, G. Graphene Induced Formation of Single Crystal Pt Nanosheets through 2-Dimensional Aggregation and Sintering of Nanoparticles on Molten Salt Medium. *Carbon* **2014**, *77*, 1123–1131. [CrossRef]
109. Yang, C.; Wang, T.; Wang, T.; He, H.; Liu, D.; Huang, H. Ultrathin PdMo Bimetallene Immobilized on Graphene Nanosheets as an Efficient Bifunctional Electrocatalyst towards Formic Acid and Methanol Oxidation Reactions. *Int. J. Hydrogen Energy* **2024**, *80*, 1174–1181. [CrossRef]
110. He, C.; Tao, J.; Shen, P.K. Solid Synthesis of Ultrathin Palladium and Its Alloys' Nanosheets on RGO with High Catalytic Activity for Oxygen Reduction Reaction. *ACS Catal.* **2018**, *8*, 910–919. [CrossRef]
111. Zhang, Q.; Jiang, Q.; Yang, X.; Zhang, C.; Zhang, J.; Yang, L.; He, H.; Ying, G.; Huang, H. Heterointerface Engineering of Rhombic Rh Nanosheets Confined on MXene for Efficient Methanol Oxidation. *J. Energy Chem.* **2024**, *93*, 419–428. [CrossRef]
112. Huang, H.; Xiao, D.; Zhu, Z.; Zhang, C.; Yang, L.; He, H.; You, J.; Jiang, Q.; Xu, X.; Yamauchi, Y. A 2D/2D Heterojunction of Ultrathin Pd Nanosheet/MXene towards Highly Efficient Methanol Oxidation Reaction: The Significance of 2D Material Nanoarchitectonics. *Chem. Sci.* **2023**, *14*, 9854–9862. [CrossRef]
113. Xiong, J.; Wang, Y.; Yang, C.; Yang, L.; Zhang, C.; Jiang, Q.; He, H.; Ying, G.; Huang, H. Confining Rhodium Nanocrystals into Polyaniline Nanorod-Embedded MXene Nanoarchitectures Enables Efficient Methanol Electrooxidation. *J. Colloid Interface Sci.* **2025**, *695*, 137809. [CrossRef]
114. Lan, Y.; He, H.; Liu, C.; Qin, J.; Luo, L.; Zhu, F.; Zhao, Y.; Zhang, J.; Yang, L.; Huang, H. Ultrasmall Pd Nanocrystals Confined into Co-Based Metal Organic Framework-Decorated MXene Nanoarchitectures for Efficient Methanol Electrooxidation. *J. Power Sources* **2024**, *603*, 234438. [CrossRef]
115. Qin, J.; Huang, H.; Zhang, J.; Zhu, F.; Luo, L.; Zhang, C.; Yang, L.; Jiang, Q.; He, H. Stereoassembly of Ultrasmall Rh-Decorated Zeolite Imidazolate Framework–MXene Heterostructures for Boosted Methanol Oxidation Reaction. *J. Mater. Chem. A* **2023**, *11*, 2848–2856. [CrossRef]
116. Zhang, L.Y.; Zeng, T.; Zheng, L.; Wang, Y.; Yuan, W.; Niu, M.; Guo, C.X.; Cao, D.; Li, C.M. Epitaxial Growth of Pt–Pd Bimetallic Heterostructures for the Oxygen Reduction Reaction. *Adv. Powder Mater.* **2023**, *2*, 100131. [CrossRef]
117. Li, J.; Wang, C.; Zhang, Y.; Hata, S.; Zhang, K.; Ye, C.; Shiraishi, Y.; Du, Y. Advanced Heterostructure of Pd Nanosheets@Pt Nanoparticles Boosts Methanol Electrooxidation. *J. Energy Chem.* **2023**, *85*, 430–438. [CrossRef]

118. Ding, J.; Wang, F.; Pan, F.; Yu, P.; Gao, N.; Goldsmith, R.H.; Cai, S.; Yang, R.; He, J. Two-Dimensional Palladium Nanosheet Intercalated with Gold Nanoparticles for Plasmon-Enhanced Electrocatalysis. *ACS Catal.* **2021**, *11*, 13721–13732. [CrossRef]
119. Xie, Y.; Zhang, S.; Shen, B.; He, H.; Huang, H. Confining Tungsten Disulfide Quantum Dots on MXene Nanosheets Enables Efficient Hydrogen Evolution Reaction. *ACS Appl. Energy Mater.* **2025**, *8*, 2747–2754. [CrossRef]
120. Ma, C.; He, H.; Qin, J.; Luo, L.; Lan, Y.; Zhang, J.; Yang, L.; Jiang, Q.; Huang, H. The Marriage of Hydrazone-Linked Covalent Organic Frameworks and MXene Enables Efficient Electrocatalytic Hydrogen Evolution. *Small Struct.* **2023**, *5*, 2300279. [CrossRef]
121. Ma, C.; He, H.; Qin, J.; Hao, L.; Jia, L.; Yang, L.; Huang, H. Combining MXene Nanosheets with Iron-Based Metal-Organic Frameworks for Enhanced Electrocatalytic Hydrogen Evolution Reaction. *Mater. Today Chem.* **2023**, *30*, 101531. [CrossRef]
122. He, H.; Chen, Y.; Yang, C.; Yang, L.; Jiang, Q.; Huang, H. Constructing 3D Interweaved MXene/Graphitic Carbon Nitride Nanosheets/Graphene Nanoarchitectures for Promoted Electrocatalytic Hydrogen Evolution. *J. Energy Chem.* **2022**, *67*, 483–491. [CrossRef]
123. Luo, L.; Meng, W.; Wang, G.; Qin, J.; He, H.; Huang, H. MnO_2 Nanoflowers-Decorated MXene Nanosheets with Enhanced Supercapacitor Performance. *J. Alloys Compd.* **2023**, *957*, 170411. [CrossRef]
124. Chen, Z.; Duan, X.; Wei, W.; Wang, S.; Ni, B.-J. Iridium-Based Nanomaterials for Electrochemical Water Splitting. *Nano Energy* **2020**, *78*, 105270. [CrossRef]
125. Zhang, B.; Zheng, Y.; Ma, T.; Yang, C.; Peng, Y.; Zhou, Z.; Zhou, M.; Li, S.; Wang, Y.; Cheng, C. Designing MOF Nanoarchitectures for Electrochemical Water Splitting. *Adv. Mater.* **2021**, *33*, 2006042. [CrossRef]
126. Hao, L.; He, H.; Xu, C.; Zhang, M.; Feng, H.; Yang, L.; Jiang, Q.; Huang, H. Ultrafine Cobalt Selenide Nanowires Tangled with MXene Nanosheets as Highly Efficient Electrocatalysts toward the Hydrogen Evolution Reaction. *Dalton Trans.* **2022**, *51*, 7135–7141. [CrossRef]
127. Zhou, F.; Zhou, Y.; Liu, G.-G.; Wang, C.-T.; Wang, J. Recent Advances in Nanostructured Electrocatalysts for Hydrogen Evolution Reaction. *Rare Met.* **2021**, *40*, 3375–3405. [CrossRef]
128. Araújo, H.F.; Gómez, J.A.; Santos, D.M.F. Proton-Exchange Membrane Electrolysis for Green Hydrogen Production: Fundamentals, Cost Breakdown, and Strategies to Minimize Platinum-Group Metal Content in Hydrogen Evolution Reaction Electrocatalysts. *Catalysts* **2024**, *14*, 845. [CrossRef]
129. Hua, W.; Sun, H.-H.; Xu, F.; Wang, J.-G. A Review and Perspective on Molybdenum-Based Electrocatalysts for Hydrogen Evolution Reaction. *Rare Met.* **2020**, *39*, 335–351. [CrossRef]
130. Li, T.; Dong, Y.; Zhang, J.; Wang, L.; Duan, F.; Wang, D.; Zeng, H. Carbon Dots-Based Composites Electrocatalysts in Hydrogen Evolution Reaction and Oxygen Evolution Reaction: A Mini Review. *Int. J. Hydrogen Energy* **2024**, *77*, 359–372. [CrossRef]
131. Fan, J.; Wu, J.; Cui, X.; Gu, L.; Zhang, Q.; Meng, F.; Lei, B.-H.; Singh, D.J.; Zheng, W. Hydrogen Stabilized RhPdH 2D Bimetallene Nanosheets for Efficient Alkaline Hydrogen Evolution. *J. Am. Chem. Soc.* **2020**, *142*, 3645–3651. [CrossRef]
132. Lin, B.-L.; Chen, X.; Niu, B.-T.; Lin, Y.-T.; Chen, Y.-X.; Lin, X.-M. The Research Progress of Ruthenium-Based Catalysts for the Alkaline Hydrogen Evolution Reaction in Water Electrolysis. *Catalysts* **2024**, *14*, 671. [CrossRef]
133. Shen, B.; Huang, H.; Jiang, Y.; Xue, Y.; He, H. 3D Interweaving MXene–Graphene Network–Confined Ni–Fe Layered Double Hydroxide Nanosheets for Enhanced Hydrogen Evolution. *Electrochim. Acta* **2022**, *407*, 139913. [CrossRef]
134. Huang, H.; Xue, Y.; Xie, Y.; Yang, Y.; Yang, L.; He, H.; Jiang, Q.; Ying, G. MoS_2 Quantum Dot-Decorated MXene Nanosheets as Efficient Hydrogen Evolution Electrocatalysts. *Inorg. Chem. Front.* **2022**, *9*, 1171–1178. [CrossRef]
135. Xue, Y.; Xie, Y.; Xu, C.; He, H.; Jiang, Q.; Ying, G.; Huang, H. 0D/2D Heterojunction of Graphene Quantum Dots/MXene Nanosheets for Boosted Hydrogen Evolution Reaction. *Surf. Interfaces* **2022**, *30*, 101907. [CrossRef]
136. Hansen, J.N.; Prats, H.; Toudahl, K.K.; Mørch Secher, N.; Chan, K.; Kibsgaard, J.; Chorkendorff, I. Is There Anything Better than Pt for HER? *ACS Energy Lett.* **2021**, *6*, 1175–1180. [CrossRef]
137. Guo, F.; Macdonald, T.J.; Sobrido, A.J.; Liu, L.; Feng, J.; He, G. Recent Advances in Ultralow-Pt-Loading Electrocatalysts for the Efficient Hydrogen Evolution. *Adv. Sci.* **2023**, *10*, e2301098. [CrossRef]
138. Hao, L.; He, H.; Qin, J.; Ma, C.; Luo, L.; Yang, L.; Huang, H. MXene Nanosheets Induce Efficient Iron Selenide Active Sites to Boost the Electrocatalytic Hydrogen Evolution Reaction. *Inorg. Chem.* **2022**, *61*, 21087–21094. [CrossRef]
139. Zhao, Y.; Cong, H.; Li, P.; Wu, D.; Chen, S.; Luo, W. Hexagonal $RuSe_2$ Nanosheets for Highly Efficient Hydrogen Evolution Electrocatalysis. *Angew. Chem. Int. Ed.* **2021**, *60*, 7013–7017. [CrossRef]
140. Ma, C.; Chen, W.; Wu, Y.; Wang, W.; Xu, L.; Chen, C.; Zheng, L.; Wang, G.; Han, P.; Gu, P.; et al. Undercoordinated Two-Dimensional Pt Nanoring Stabilized by a Ring-on-Sheet Nanoheterostructure for Highly Efficient Alkaline Hydrogen Evolution Reaction. *Nano Lett.* **2025**, *25*, 3212–3220. [CrossRef]
141. Zhang, D.; Zhao, H.; Huang, B.; Li, B.; Li, H.; Han, Y.; Wang, Z.; Wu, X.; Pan, Y.; Sun, Y.; et al. Advanced Ultrathin RuPdM (M = Ni, Co, Fe) Nanosheets Electrocatalyst Boosts Hydrogen Evolution. *ACS Cent. Sci.* **2019**, *5*, 1991–1997. [CrossRef]
142. Cai, C.; Liu, K.; Zhu, Y.; Li, P.; Wang, Q.; Liu, B.; Chen, S.; Li, H.; Zhu, L.; Li, H.; et al. Optimizing Hydrogen Binding on Ru Sites with RuCo Alloy Nanosheets for Efficient Alkaline Hydrogen Evolution. *Angew. Chem. Int. Ed.* **2022**, *61*, e202113664. [CrossRef]

143. Lv, F.; Huang, B.; Feng, J.; Zhang, W.; Wang, K.; Li, N.; Zhou, J.; Zhou, P.; Yang, W.; Du, Y.; et al. A Highly Efficient Atomically Thin Curved PdIr Bimetallene Electrocatalyst. *Natl. Sci. Rev.* **2021**, *8*, nwab019. [CrossRef]
144. Jin, X.; Kwon, S.J.; Kim, M.G.; Kim, M.; Hwang, S.-J. Crucial Role of Metal Coordination Number in Optimizing Electrocatalyst Activity of Holey Large-Area 2D Ru Nanosheets. *ACS Nano* **2024**, *18*, 15194–15203. [CrossRef]
145. Wang, L.; Zeng, Z.; Gao, W.; Maxson, T.; Raciti, D.; Giroux, M.; Pan, A.; Wang, C.; Greeley, J. Tunable Intrinsic Strain in Two-Dimensional Transition Metal Electrocatalysts. *Science* **2019**, *363*, 870–874. [CrossRef]
146. Huo, J.; Dou, Y.; Wu, C.; Liu, H.; Dou, S.; Yuan, D. Defect Engineering of Metal-Based Atomically Thin Materials for Catalyzing Small-Molecule Conversion Reactions. *Adv. Mater.* **2025**, *37*, e2416483. [CrossRef]
147. Li, Q.; Kudo, A.; Ma, J.; Kawashima, R.; Toyama, K.; Xu, W.; Gao, Z.; Liang, Y.; Jiang, H.; Li, Z.; et al. Tuning Electrocatalytic Activities of Dealloyed Nanoporous Catalysts by Macroscopic Strain Engineering. *Nano Lett.* **2024**, *24*, 5543–5549. [CrossRef]
148. Zhao, C.; Shu, C.; Zheng, R.; Du, D.; Ren, L.; He, M.; Li, R.; Xu, H.; Wen, X.; Long, J. Adjusting the D-Band Center of Metallic Sites in NiFe-Based Bimetal-Organic Frameworks via Tensile Strain to Achieve High-Performance Oxygen Electrode Catalysts for Lithium-Oxygen Batteries. *J. Colloid Interface Sci.* **2022**, *607*, 1215–1225. [CrossRef]
149. Xia, Z.; Guo, S. Strain Engineering of Metal-Based Nanomaterials for Energy Electrocatalysis. *Chem. Soc. Rev.* **2019**, *48*, 3265–3278. [CrossRef]
150. Guan, C.; Yue, X.; Xiang, Q. The Role of Lattice Distortion in Catalysis: Functionality and Distinctions from Strain. *Adv. Mater.* 2025, *ahead of print*. [CrossRef]
151. Hou, Z.; Cui, C.; Li, Y.; Gao, Y.; Zhu, D.; Gu, Y.; Pan, G.; Zhu, Y.; Zhang, T. Lattice-Strain Engineering for Heterogenous Electrocatalytic Oxygen Evolution Reaction. *Adv. Mater.* **2023**, *35*, e2209876. [CrossRef]
152. Kari, J.; Olsen, J.P.; Jensen, K.; Badino, S.F.; Krogh, K.B.R.M.; Borch, K.; Westh, P. Sabatier Principle for Interfacial (Heterogeneous) Enzyme Catalysis. *ACS Catal.* **2018**, *8*, 11966–11972. [CrossRef]
153. Yin, S.; Liu, S.; Wang, Z.; Xu, Y.; Li, X.; Wang, H.; Wang, L. Methanol-Assisted Energy-Saving Hydrogen Production over Defect-Rich Perforated PdIn Bimetallene. *Chem. Eng. J.* **2022**, *435*, 134711. [CrossRef]
154. Ding, H.; Liu, H.; Chu, W.; Wu, C.; Xie, Y. Structural Transformation of Heterogeneous Materials for Electrocatalytic Oxygen Evolution Reaction. *Chem. Rev.* **2021**, *121*, 13174–13212. [CrossRef]
155. Wei, H.; Wang, Q.; Zhang, Y.; Li, J.; Liu, P.; Wang, N.; Gong, X. Engineering High-Entropy Alloy Nanosheets toward Efficient Electrocatalytic Water Oxidation. *Fuel* **2024**, *358*, 130011. [CrossRef]
156. Lu, X.; Xue, H.; Gong, H.; Bai, M.; Tang, D.; Ma, R.; Sasaki, T. 2D Layered Double Hydroxide Nanosheets and their Derivatives toward Efficient Oxygen Evolution Reaction. *Nano-Micro Lett.* **2020**, *12*, 86. [CrossRef]
157. Suen, N.-T.; Hung, S.-F.; Quan, Q.; Zhang, N.; Xu, Y.-J.; Chen, H.M. Electrocatalysis for the Oxygen Evolution Reaction: Recent Development and Future Perspectives. *Chem. Soc. Rev.* **2017**, *46*, 337–365. [CrossRef]
158. Xie, X.; Du, L.; Yan, L.; Park, S.; Qiu, Y.; Sokolowski, J.; Wang, W.; Shao, Y. Oxygen Evolution Reaction in Alkaline Environment: Material Challenges and Solutions. *Adv. Funct. Mater.* **2022**, *32*, 2110036. [CrossRef]
159. Mo, J.; Fu, N.; Mu, S.; Peng, J.; Liu, Y.; Zhang, G. Facile Synthesis of Metal/Carbide Hybrid toward Overall Water Splitting. *Catalysts* **2024**, *14*, 730. [CrossRef]
160. Shen, B.; Feng, Y.; Wang, Y.; Sun, P.; Yang, L.; Jiang, Q.; He, H.; Huang, H. Holey MXene Nanosheets Intimately Coupled with Ultrathin Ni–Fe Layered Double Hydroxides for Boosted Hydrogen and Oxygen Evolution Reactions. *Carbon* **2023**, *212*, 118141. [CrossRef]
161. He, L.; Tang, Q.; Fan, Q.; Zhuang, H.; Wang, S.; Pang, Y.; Liang, K. Vertically Ti_3CN@NiFe LDH Nanoflakes as Self-Standing Catalysts for Enhanced Oxygen Evolution Reaction. *Catalysts* **2024**, *14*, 708. [CrossRef]
162. Song, Y.; Chen, H.; Wang, X.; Weng, C.; Zou, K.; Wang, C.; Yuan, Y.; Ma, Y.; Yang, X.; Lin, W. Engineering Ir-based Catalysts for High Current Density Applications in Proton Exchange Membrane Water Electrolyzers. *Energy Environ. Sci.* **2025**, *18*, 130–154. [CrossRef]
163. Gao, G.; Sun, Z.; Chen, X.; Zhu, G.; Sun, B.; Yamauchi, Y.; Liu, S. Recent Advances in Ru/Ir-Based Electrocatalysts for Acidic Oxygen Evolution Reaction. *Appl. Catal. B Environ.* **2024**, *343*, 123584. [CrossRef]
164. Wang, H.; Li, X.; Zhang, G.; Gu, Z.; Chen, H.; Wei, G.; Shen, S.; Cheng, J.; Zhang, J. Recent Progress in Balancing the Activity, Durability, and Low Ir Content for Ir-Based Oxygen Evolution Reaction Electrocatalysts in Acidic Media. *Small* **2024**, *21*, 2410407. [CrossRef]
165. Thao, N.T.T.; Jang, J.U.; Nayak, A.K.; Han, H. Current Trends of Iridium-Based Catalysts for Oxygen Evolution Reaction in Acidic Water Electrolysis. *Small Sci.* **2024**, *4*, 2300109. [CrossRef]
166. Yu, H.; Ke, J.; Shao, Q. Two Dimensional Ir-Based Catalysts for Acidic OER. *Small* **2023**, *19*, e2304307. [CrossRef]
167. Chen, H.; Shi, L.; Sun, K.; Zhang, K.; Liu, Q.; Ge, J.; Liang, X.; Tian, B.; Huang, Y.; Shi, Z.; et al. Protonated Iridate Nanosheets with a Highly Active and Stable Layered Perovskite Framework for Acidic Oxygen Evolution. *ACS Catal.* **2022**, *12*, 8658–8666. [CrossRef]

168. Jiang, B.; Guo, Y.; Kim, J.; Whitten, A.E.; Wood, K.; Kani, K.; Rowan, A.E.; Henzie, J.; Yamauchi, Y. Mesoporous Metallic Iridium Nanosheets. *J. Am. Chem. Soc.* **2018**, *140*, 12434–12441. [CrossRef]
169. Chatterjee, S.; Peng, X.; Intikhab, S.; Zeng, G.; Kariuki, N.N.; Myers, D.J.; Danilovic, N.; Snyder, J. Nanoporous Iridium Nanosheets for Polymer Electrolyte Membrane Electrolysis. *Adv. Energy Mater.* **2021**, *11*, 2101438. [CrossRef]
170. Zhu, L.; Ma, C.; Li, D.; Shao, X.; Cao, L.; Yang, J. Designing of Hexagonal Nanosheets with Edge-Sharing [IrO_6] Octahedral Crystals for Efficient and Stable Acidic Water Splitting. *Adv. Funct. Mater.* **2023**, *34*, 2313375. [CrossRef]
171. Kong, X.; Xu, K.; Zhang, C.; Dai, J.; Norooz Oliaee, S.; Li, L.; Zeng, X.; Wu, C.; Peng, Z. Free-Standing Two-Dimensional Ru Nanosheets with High Activity toward Water Splitting. *ACS Catal.* **2016**, *6*, 1487–1492. [CrossRef]
172. Chen, F.-Y.; Wu, Z.-Y.; Adler, Z.; Wang, H. Stability Challenges of Electrocatalytic Oxygen Evolution Reaction: From Mechanistic Understanding to Reactor Design. *Joule* **2021**, *5*, 1704–1731. [CrossRef]
173. Minke, C.; Suermann, M.; Bensmann, B.; Hanke-Rauschenbach, R. Is Iridium Demand a Potential Bottleneck in the Realization of Large-Scale Pem Water Electrolysis? *Int. J. Hydrogen Energy* **2021**, *46*, 23581–23590. [CrossRef]
174. Li, S.; Zhao, S.; Hu, F.; Li, L.; Ren, J.; Jiao, L.; Ramakrishna, S.; Peng, S. Exploring the Potential Ru-Based Catalysts for Commercial-Scale Polymer Electrolyte Membrane Water Electrolysis: A Systematic Review. *Prog. Mater. Sci.* **2024**, *145*, 101294. [CrossRef]
175. Qin, R.; Chen, G.; Feng, X.; Weng, J.; Han, Y. Ru/Ir-Based Electrocatalysts for Oxygen Evolution Reaction in Acidic Conditions: From Mechanisms, Optimizations to Challenges. *Adv. Sci.* **2024**, *11*, e2309364. [CrossRef]
176. Yuan, J.H.; Li, L.H.; Zhang, W.; Xue, K.H.; Wang, C.; Wang, J.; Miao, X.S.; Zeng, X.C. Pt_5Se_4 Monolayer: A Highly Efficient Electrocatalyst toward Hydrogen and Oxygen Electrode Reactions. *ACS Appl. Mater. Interfaces* **2020**, *12*, 13896–13903. [CrossRef]
177. Zhang, J.; Yuan, Y.; Gao, L.; Zeng, G.; Li, M.; Huang, H. Stabilizing Pt-Based Electrocatalysts for Oxygen Reduction Reaction: Fundamental Understanding and Design Strategies. *Adv. Mater.* **2021**, *33*, e2006494. [CrossRef]
178. Tian, X.; Lu, X.F.; Xia, B.Y.; Lou, X.W. Advanced Electrocatalysts for the Oxygen Reduction Reaction in Energy Conversion Technologies. *Joule* **2020**, *4*, 45–68. [CrossRef]
179. Chen, J.W.; Zhang, Z.; Yan, H.M.; Xia, G.J.; Cao, H.; Wang, Y.G. Pseudo-Adsorption and Long-Range Redox Coupling During Oxygen Reduction Reaction on Single Atom Electrocatalyst. *Nat. Commun.* **2022**, *13*, 1734. [CrossRef]
180. Ao, X.; Wang, H.; Zhang, X.; Wang, C. Atomically Dispersed Metal-Nitrogen-Carbon Catalysts for Acidic Oxygen Reduction Reaction. *ACS Appl. Mater. Interfaces* **2025**, *17*, 2844–2862. [CrossRef]
181. Yu, J.; Su, C.; Shang, L.; Zhang, T. Single-Atom-Based Oxygen Reduction Reaction Catalysts for Proton Exchange Membrane Fuel Cells: Progress and Perspective. *ACS Nano* **2023**, *17*, 19514–19525. [CrossRef]
182. Luo, J.; Zhang, Y.; Lu, Z.; Liu, C.; Xu, Y.; Chen, H.; Wang, Q.; Wu, D.; Dang, D.; Deng, Y.; et al. Oxygen-Coordinated Cr Single-Atom Catalyst for Oxygen Reduction Reaction in Proton Exchange Membrane Fuel Cells. *Angew. Chem. Int. Ed.* **2025**, *64*, e202500500. [CrossRef]
183. Pruchyathamkorn, J.; Yang, M.; Amin, H.M.A.; Batchelor-McAuley, C.; Compton, R.G. Imaging Electrode Heterogeneity Using Chemically Confined Fluorescence Electrochemical Microscopy. *J. Phys. Chem. Lett.* **2017**, *8*, 6124–6127. [CrossRef]
184. Pan, L.; Merzdorf, T.; Campos-Roldàn, C.A.; Guo, A.; Lu, J.; Schmidt, J.; Heggen, M.; Klingenhof, M.; Wang, X.; Möhle, S.; et al. From Seeds to Cell: Improving PEMFC Performance and Durability by Seed-Mediation Synthesis for PtNiIr ORR Nanocatalysts. *Adv. Sci.* 2025, *ahead of print*. [CrossRef]
185. Chen, Y.; Huang, Z.; Yu, J.; Wang, H.; Qin, Y.; Xing, L.; Du, L. Research Progress of Pt-Based Catalysts toward Cathodic Oxygen Reduction Reactions for Proton Exchange Membrane Fuel Cells. *Catalysts* **2024**, *14*, 569. [CrossRef]
186. Banham, D.; Ye, S. Current Status and Future Development of Catalyst Materials and Catalyst Layers for Proton Exchange Membrane Fuel Cells: An Industrial Perspective. *ACS Energy Lett.* **2017**, *2*, 629–638. [CrossRef]
187. Sinniah, J.D.; Wong, W.Y.; Loh, K.S.; Yunus, R.M.; Timmiati, S.N. Perspectives on Carbon-Alternative Materials as Pt Catalyst Supports for a Durable Oxygen Reduction Reaction in Proton Exchange Membrane Fuel Cells. *J. Power Sources* **2022**, *534*, 231422. [CrossRef]
188. Amin, H.M.A.; Baltruschat, H.; Wittmaier, D.; Friedrich, K.A. A Highly Efficient Bifunctional Catalyst for Alkaline Air-Electrodes Based on a Ag and Co_3O_4 Hybrid: RRDE and Online DEMS Insights. *Electrochim. Acta* **2015**, *151*, 332–339. [CrossRef]
189. Amin, H.M.A.; Konigshoven, P.; Hegemann, M.; Baltruschat, H. Role of Lattice Oxygen in the Oxygen Evolution Reaction on Co_3O_4: Isotope Exchange Determined Using a Small-Volume Differential Electrochemical Mass Spectrometry Cell Design. *Anal. Chem.* **2019**, *91*, 12653–12660. [CrossRef]
190. Liang, J.; Li, S.; Chen, Y.; Liu, X.; Wang, T.; Han, J.; Jiao, S.; Cao, R.; Li, Q. Ultrathin and Defect-Rich Intermetallic Pd_2Sn Nanosheets for Efficient Oxygen Reduction Electrocatalysis. *J. Mater. Chem. A* **2020**, *8*, 15665–15669. [CrossRef]
191. Chen, Q.; Chen, Z.; Ali, A.; Luo, Y.; Feng, H.; Luo, Y.; Tsiakaras, P.; Kang Shen, P. Shell-Thickness-Dependent Pd@Ptni Core–Shell Nanosheets for Efficient Oxygen Reduction Reaction. *Chem. Eng. J.* **2022**, *427*, 131565. [CrossRef]
192. Zhang, S.; Liu, S.; Cao, W.; Luo, J.; Gu, Y.; Liu, X.; Tan, P.; Wang, Z.; Pan, J. Microwave Heating-Assisted Synthesis of Ultrathin Platinum-Based Trimetallic Nanosheets as Highly Stable Catalysts towards Oxygen Reduction Reaction in Acidic Medium. *J. Colloid Interface Sci.* **2024**, *675*, 1108–1118. [CrossRef]

193. Peng, X.; Lu, D.; Qin, Y.; Li, M.; Guo, Y.; Guo, S. Pt-on-Pd Dendritic Nanosheets with Enhanced Bifunctional Fuel Cell Catalytic Performance. *ACS Appl. Mater. Interfaces* **2020**, *12*, 30336–30342. [CrossRef]
194. Zhang, L.Y.; Guo, C.X.; Cao, H.; Wang, S.; Ouyang, Y.; Xu, B.; Guo, P.; Li, C.M. Highly Wrinkled Palladium Nanosheets as Advanced Electrocatalysts for the Oxygen Reduction Reaction in Acidic Medium. *Chem. Eng. J.* **2022**, *431*, 133237. [CrossRef]
195. Chen, W.; Gao, W.; Tu, P.; Robert, T.; Ma, Y.; Shan, H.; Gu, X.; Shang, W.; Tao, P.; Song, C.; et al. Neighboring Pt Atom Sites in an Ultrathin FePt Nanosheet for the Efficient and Highly CO-Tolerant Oxygen Reduction Reaction. *Nano Lett.* **2018**, *18*, 5905–5912. [CrossRef]
196. Li, Y.; Yao, M.S.; He, Y.; Du, S. Recent Advances of Electrocatalysts and Electrodes for Direct Formic Acid Fuel Cells: From Nano to Meter Scale Challenges. *Nano-Micro Lett.* **2025**, *17*, 148. [CrossRef]
197. Al-Nayili, A.; Majdi, H.S.; Albayati, T.M.; Saady, N.M.C. Formic Acid Dehydrogenation Using Noble-Metal Nanoheterogeneous Catalysts: Towards Sustainable Hydrogen-Based Energy. *Catalysts* **2022**, *12*, 324. [CrossRef]
198. Guo, X.; Yang, L.; Shen, B.; Wei, Y.; Yang, Y.; Yang, C.; Jiang, Q.; He, H.; Huang, H. Ultrafine Pd Nanocrystals Anchored onto Single-Walled Carbon Nanohorns: A Highly-Efficient Multifunctional Electrocatalyst with Ultra-Low Pd Loading for Formic Acid and Methanol Oxidation. *Mater. Chem. Phys.* **2020**, *250*, 123167. [CrossRef]
199. Zheng, J.-H.; Zhang, J.; Li, G.; Zhang, J.-M.; Zhang, B.-W.; Jiang, Y.-X.; Sun, S.-G. Tuning Atomic Pt Site Surface on Ptau Alloy toward Electro-Oxidation of Formic Acid. *Mater. Today Energy* **2022**, *27*, 101028. [CrossRef]
200. Hu, X.; Xiao, Z.; Wang, W.; Bu, L.; An, Z.; Liu, S.; Pao, C.W.; Zhan, C.; Hu, Z.; Yang, Z.; et al. Platinum-Lead-Bismuth/Platinum-Bismuth Core/Shell Nanoplate Achieves Complete Dehydrogenation Pathway for Direct Formic Acid Oxidation Catalysis. *J. Am. Chem. Soc.* **2023**, *145*, 15109–15117. [CrossRef]
201. Zhang, Y.; Qiao, M.; Huang, Y.; Zou, Y.; Liu, Z.; Tao, L.; Li, Y.; Dong, C.L.; Wang, S. In Situ Exfoliation and Pt Deposition of Antimonene for Formic Acid Oxidation via a Predominant Dehydrogenation Pathway. *Research* **2020**, *2020*, 5487237. [CrossRef]
202. Hu, X.; An, Z.; Wang, W.; Lin, X.; Chan, T.S.; Zhan, C.; Hu, Z.; Yang, Z.; Huang, X.; Bu, L. Sub-Monolayer SbO_x on PtPb/Pt Nanoplate Boosts Direct Formic Acid Oxidation Catalysis. *J. Am. Chem. Soc.* **2023**, *145*, 19274–19282. [CrossRef]
203. Ge, Z.-X.; Miao, B.-Q.; Tian, X.-L.; He, B.; Chen, Y. Chemical Functionalization of Commercial Pt/C Electrocatalyst towards Formic Acid Electrooxidation. *Chem. Eng. J.* **2023**, *476*, 146529. [CrossRef]
204. Kim, J.; Kim, H.; Kim, S.; Jang, J.-H.; Sohn, H.; Hong, S.J.; Kim, J.; Han, G.H.; Choe, S.; Sung, Y.-E.; et al. Atomic Pt clusters on Au dendrite for Formic Acid Oxidation. *Chem. Eng. J.* **2023**, *451*, 138664. [CrossRef]
205. Dong, C.; Zhang, B.; Song, H.; Zhou, S.; Ye, J.; Liao, H.-G.; Dong, L.; Huang, X.; Bu, L. Platinum–Tellurium Heterojunction Nanosheet Assemblies for Efficient Direct Formic Acid Electrooxidation Catalysis. *ACS Nano* **2024**, *18*, 10008–10018. [CrossRef]
206. Liu, L.; Jin, L.; Xiao, Z.; Fang, N.; Lin, X.; Ji, Y.; Wang, Y.; Li, Y.; Huang, X.; Bu, L. Heterostructured Pt-PbS Nanobelt Achieves Remarkable Direct Formic Acid Oxidation Catalysis. *Nano Lett.* **2024**, *24*, 8162–8170. [CrossRef]
207. Zhou, Y.-W.; Chen, Y.-F.; Qin, X.; Jiang, K.; Lin, W.-F.; Cai, W.-B. Boosting Electrocatalytic Oxidation of Formic Acid on SnO_2-Decorated Pd Nanosheets. *J. Catal.* **2021**, *399*, 8–14. [CrossRef]
208. Yang, N.; Zhang, Z.; Chen, B.; Huang, Y.; Chen, J.; Lai, Z.; Chen, Y.; Sindoro, M.; Wang, A.L.; Cheng, H.; et al. Synthesis of Ultrathin PdCu Alloy Nanosheets Used as a Highly Efficient Electrocatalyst for Formic Acid Oxidation. *Adv. Mater.* **2017**, *29*, 1700768. [CrossRef]
209. Wei, J.; Wu, F.; Sun, H.; Xia, S.; Sang, X.; Li, F.; Zhang, Z.; Han, S.; Niu, W. Modulate the Metallic Sb State on Ultrathin PdSb-Based Nanosheets for Efficient Formic Acid Electrooxidation. *J. Colloid Interface Sci.* **2023**, *648*, 473–480. [CrossRef]
210. Ahmadi, A.; Ebrahimifar, H.; Askari, M.B. Alcohol Electrooxidation on Three-Component NiO/La_2O_3/MWCNTs Catalyst for DAFC Application. *Electrochem. Commun.* **2025**, *176*, 107963. [CrossRef]
211. Wu, F.; Zeng, L.; Zhu, L.; Wang, W.; Cao, C.; Yang, Z.; Shang, C.; Ye, H.; Guo, Z. Cooperative Pd@CoNi/rG Catalyst for Highly Efficient and Stable Electrocatalytic Methanol and Ethanol Oxidations. *Chem. Eng. J.* **2024**, *502*, 158010. [CrossRef]
212. Guo, X.; Xiong, J.; Wang, Q.; Zhang, J.; He, H.; Huang, H. Ultrafine Rh Nanocrystals Grown onto a Boron and Nitrogen Codoped Carbon Support with a Horn-Shaped Structure for Highly Efficient Methanol Oxidation. *Dalton Trans.* **2022**, *51*, 16982–16989. [CrossRef]
213. Ren, J.; Zhang, J.; Yang, C.; Yang, Y.; Zhang, Y.; Yang, F.; Ma, R.; Yang, L.; He, H.; Huang, H. Pd Nanocrystals Anchored on 3D Hybrid Architectures Constructed from Nitrogen-Doped Graphene and Low-Defect Carbon Nanotube as High-Performance Multifunctional Electrocatalysts for Formic Acid and Methanol Oxidation. *Mater. Today Energy* **2020**, *16*, 100409. [CrossRef]
214. Zhang, Q.; Li, Y.; He, H.; Huang, H. Building 3D Interconnected MoS_2 Nanosheet–Graphene Networks Decorated with Rh Nanoparticles for Boosted Methanol Oxidation Reaction. *ACS Sustain. Chem. Eng.* **2022**, *10*, 8940–8948. [CrossRef]
215. Guo, X.; Zhang, Q.; Li, Y.; Chen, Y.; Yang, L.; He, H.; Xu, X.; Huang, H. Nanosized Rh Grown on Single-Walled Carbon Nanohorns for Efficient Methanol Oxidation Reaction. *Rare Met.* **2022**, *41*, 2108–2117. [CrossRef]
216. Guo, X.; Wang, Q.; He, H.; Huang, H. Boron and Nitrogen Codoped Carbon Nanohorn-Supported Pt Nanocrystals as Highly-Efficient Methanol Oxidation Electrocatalysts. *J. Mater. Res. Technol.* **2022**, *19*, 722–731. [CrossRef]

217. Berretti, E.; Osmieri, L.; Baglio, V.; Miller, H.A.; Filippi, J.; Vizza, F.; Santamaria, M.; Specchia, S.; Santoro, C.; Lavacchi, A. Direct Alcohol Fuel Cells: A Comparative Review of Acidic and Alkaline Systems. *Electrochem. Energy Rev.* **2023**, *6*, 30. [CrossRef]
218. Elsaid, K.; Abdelfatah, S.; Abdel Elabsir, A.M.; Hassiba, R.J.; Ghouri, Z.K.; Vechot, L. Direct Alcohol Fuel Cells: Assessment of the Fuel's Safety and Health Aspects. *Int. J. Hydrogen Energy* **2021**, *46*, 30658–30668. [CrossRef]
219. Yu, Y.; Wang, T.; Jiang, X.; Chen, K.; Wu, Q.; Zhang, Y.; Shi, D.; Li, H. Advances in the Preparation Strategies and Structural Regulation for CeO_2-Containing Electrocatalysts Applied to the Anodes of Direct Alcohol Fuel Cells: A Comprehensive Review. *J. Mater. Chem. A* **2025**, *13*, 20143–20175. [CrossRef]
220. Mohammadi, T.; Hosseini, M.G.; Diaz-Coello, S.; Pastor, E.; Ahadzadeh, I. Monitoring of Ethanol Electrooxidation on Highly Efficient Conductive Runi Metal-Organic Framework by Mass Spectrometry. *J. Power Sources* **2024**, *611*, 234758. [CrossRef]
221. Xue, Y.; Xiong, J.; Zhang, H.; He, H.; Huang, H. Ultrafine Rh Nanocrystals Immobilized on 3D Boron and Nitrogen Co-Doped Graphene–Carbon Nanotube Networks: High-Efficiency Electrocatalysts towards the Methanol Oxidation Reaction. *Catal. Sci. Technol.* **2022**, *12*, 6016–6023. [CrossRef]
222. Qiang, L.; Wen, W.; Yan, Q.; Zhao, P.; Ma, J.; Liu, C.; Zhao, M.; He, Y.; Xiao, H.; Jia, J. Recent Advances in Constructing Efficient Electrocatalysts for Ethanol Oxidation Reaction. *J. Alloys Compd.* **2024**, *1001*, 175120. [CrossRef]
223. Ipadeola, A.K.; Eid, K.; Lebechi, A.K.; Abdullah, A.M.; Ozoemena, K.I. Porous Multi-Metallic Pt-Based Nanostructures as Efficient Electrocatalysts for Ethanol Oxidation: A Mini-Review. *Electrochem. Commun.* **2022**, *140*, 107330. [CrossRef]
224. Bai, S.; Xu, Y.; Cao, K.; Huang, X. Selective Ethanol Oxidation Reaction at the Rh-SnO_2 Interface. *Adv. Mater.* **2021**, *33*, e2005767. [CrossRef]
225. Liu, C.; Shen, Y.; Zhang, J.; Li, G.; Zheng, X.; Han, X.; Xu, L.; Zhu, S.; Chen, Y.; Deng, Y.; et al. Multiple Twin Boundary-Regulated Metastable Pd for Ethanol Oxidation Reaction. *Adv. Energy Mater.* **2022**, *12*, 2103505. [CrossRef]
226. Zhang, Y.; Liu, X.; Liu, T.; Ma, X.; Feng, Y.; Xu, B.; Cai, W.; Li, Y.; Su, D.; Shao, Q.; et al. Rhombohedral Pd–Sb Nanoplates with Pd-Terminated Surface: An Efficient Bifunctional Fuel-Cell Catalyst. *Adv. Mater.* **2022**, *34*, 2202333. [CrossRef]
227. Xu, Y.; Li, J.; Hu, M.; Wu, Z.; Du, Y. 2D Petal-Like Pdag Nanosheets Promote Efficient Electrocatalytic Oxidation of Ethanol and Methanol. *Nanoscale* **2024**, *16*, 14096–14100. [CrossRef]
228. Lan, B.; Wang, Q.-L.; Ma, Z.-X.; Wu, Y.-J.; Jiang, X.-L.; Jia, W.-S.; Zhou, C.-X.; Yang, Y.-Y. Efficient Electrochemical Ethanol-To-CO_2 Conversion at Rhodium and Bismuth Hydroxide Interfaces. *Appl. Catal. B Environ.* **2022**, *300*, 120728. [CrossRef]
229. Xue, Y.; Zhang, H.; Xiong, J.; He, H.; Huang, H. Well-Dispersive Pt Nanocrystals Anchored onto 3D Boron and Nitrogen Double-Doped Reduced Graphene Oxide–Carbon Nanotube Frameworks as Efficient Electrocatalysts for Methanol Oxidation. *J. Electroanal. Chem.* **2022**, *921*, 116705. [CrossRef]
230. Zhu, J.-Y.; Chen, S.; Xue, Q.; Li, F.-M.; Yao, H.-C.; Xu, L.; Chen, Y. Hierarchical Porous Rh Nanosheets for Methanol Oxidation Reaction. *Appl. Catal. B Environ.* **2020**, *264*, 118520. [CrossRef]
231. Meng, X.; Ouyang, Y.; Wu, H.; Huang, H.; Wang, F.; Wang, S.; Jiang, M.; Zhang, L.Y. Hierarchical Defective Palladium-Silver Alloy Nanosheets for Ethanol Electrooxidation. *J. Colloid Interface Sci.* **2021**, *586*, 200–207. [CrossRef]
232. Dong, K.; Dai, H.; Pu, H.; Zhang, T.; Wang, Y.; Deng, Y. Constructing Efficient Ternary PtTeCu Nano-Catalysts with 2D Ultrathin-Sheet Structures for Oxidation Reaction of Alcohols. *Appl. Surf. Sci.* **2023**, *609*, 155301. [CrossRef]
233. Zhang, Y.; Li, J.; Wang, C.; Liu, D.; Yu, R.; Ye, C.; Du, Y. Activable Ru-PdRu Nanosheets with Heterogeneous Interface for High-Efficiency Alcohol Oxidation Reaction. *J. Colloid Interface Sci.* **2023**, *647*, 519–527. [CrossRef]
234. Ji, L.; Che, H.; Qian, N.; Li, J.; Luo, S.; Li, X.; Wu, X.; Xu, Q.; Gong, X.; Cui, X.; et al. Unconventional s-p-d Hybridization in Modulating Frontier Orbitals of Carbonaceous Radicals on PdBi Nanosheets for Efficient Ethanol Electrooxidation. *Appl. Catal. B Environ.* **2023**, *328*, 122521. [CrossRef]
235. Li, L.; Chu, M.; Song, R.; Liu, S.; Ren, G.; Xu, Y.; Wang, L.; Xu, Q.; Shao, Q.; Lu, J.; et al. CO Spillover on Ultrathin Bimetallic Rh/Rh-M Nanosheets. *Chem Catal.* **2022**, *2*, 1709–1719. [CrossRef]

Disclaimer/Publisher's Note: The statements, opinions and data contained in all publications are solely those of the individual author(s) and contributor(s) and not of MDPI and/or the editor(s). MDPI and/or the editor(s) disclaim responsibility for any injury to people or property resulting from any ideas, methods, instructions or products referred to in the content.